THE IMPACT OF TCR-CD3 AND TCR-PMHC-CD8 INTERACTION ON T CELL ACTIVATION

A Dissertation
Presented to
The Academic Faculty

by

Chenghao Ge

In Partial Fulfillment
of the Requirements for the Degree
Doctor of Philosophy in the
School of Biomedical Engineering

Georgia Institute of Technology
Emory University
August 2017

THE IMPACT OF TCR-CD3 AND TCR-PMHC-CD8 INTERACTION ON T CELL ACTIVATION

Approved by:

Dr. Cheng Zhu, Advisor
Department of Biomedical Engineering
Georgia Institute of Technology

Dr. Robert Dickson
Department of Chemistry
Georgia Institute of Technology

Dr. Krishnendu Roy
Department of Biomedical Engineering
Georgia Institute of Technology

Dr. Michelle Krogsgaard
Department of Pathology
New York University

Dr. Khalid Salaita
Department of Biomedical Engineering
Emory University

Date Approved: July 14, 2017

ACKNOWLEDGEMENTS

First and foremost, I would like to thank my advisor, Dr. Cheng Zhu, for his guidance, support, and inspiration over the years. The knowledge he has imparted on me is both valuable and lasting. I would also like to sincerely thank my committee members Dr. Michelle Krogsgaard, Dr. Robert Dickson, Dr. Khalid Salaita, and Dr. Krishnendu Roy for the valuable discussions and feedback on my thesis work.

The work presented in this thesis would not have been possible without my collaborators, Dr. Michelle Krogsgaard, Dr. Robert Dickson, Dr. Khalid Salaita, and Dr. Christopher Garcia. Their generous support and guidance have shaped this thesis in many ways. I would like to thank those who have worked with me on various projects, especially Dr. Yun Zhang, Dr. Liu Yang, and Yen-Cheng Chen, whom I truly enjoyed getting to know on a personal level.

Of course, I cannot forget the members of the Zhu Lab, both past and current. It has been an absolute pleasure knowing every one of you. I would like to thank Dr. Jack Wei Chen, Dr. Baoyu Liu and Dr. Arnold Ju, who have been my mentors and great friends since I first joined the lab. I would also like to thank Dr. Kaitao Li, Dr. Zhenhai Li, Dr. Yunfeng Chen, Dr. Ke Bai, Dr. Jinsung Hong, Dr. Sergey Pryschchep, Dr. Veronika Zarnitsyna, Dr. Hyun-Jung Lee, Dr. Loice Chingozha, Dr. Prithi Jothikumar, William Rittase, Vaclav Beranek, Paul Cardenas-Lizana, Fanyuan Zhou, Zhou Yuan, Ning Wu, Hao Zhang, Muaz Rushdi, Aaron Rosado, Jiexi Liao, and Steve Park for being wonderful colleagues who had a positive influence on me. My best memories during my graduate students would always been those moments we shared during lunch-time round table, and I am truly grateful that

this lab environment has been so welcoming and close-knit. Special thanks to Ms. Larissa Doudy, for being an awesome lab manager and treating everyone in the lab with such affection and warmth.

Last but not least, I would like to thank my family for all the support and advices throughout the years. Special thanks to my loving wife, Xiangyu Yan, whose unwavering support has propelled me through many challenges in the past few years.

TABLE OF CONTENTS

LIST OF TABLES

LIST OF FIGURES

LIST OF SYMBOLS AND ABBREVIATIONS

2D	Two dimensional
3D	Three dimensional
A_cK_a	Effective affinity
APC	Antigen presenting cell
BAP	Biotin acceptor peptide
BFP	Biomembrane Force Probe
DN	Double negative
DP	Double positive
EM	Electron microscopy
FRET	Fluorescence resonance energy transfer
IL-2	Interleukin 2
ITAM	Immunoreceptor Tyrosine-Based Activation Motif
K_a	Affinity
k_{off}	Off-rate

LCK	Lymphocyte-Specific Protein Tyrosine Kinase
mAB	Monoclonal antibody
m_l	Ligand density
m_r	Receptor density
MT	Mutant
NMR	Nuclear magnetic resonance
P_a	Probability of adhesion
P_b	Probability of bond
PBS	Phosphate buffered saline
(p)MHC	(peptide) Major Histocompatibility Complex
SA	Streptavidin
SP	Single positive
SPR	Surface Plasmon Resonance
t_c	Contact time
TCR	T-Cell receptor
WT	Wild type

ZAP-70	Zeta-chain-Associated Protein kinase 70

SUMMARY

T cells play important roles in adaptive immunity through mediating clearance of bacteria, virus, and cancer cells. T cell receptor (TCR) recognizes antigen presented on the surface of antigen presenting cells (APC) in the form of peptide major histocompatibility complex (pMHC). Based on this information, T cells must make fate decisions, such as expansion or differentiation, that are critical to proper T-cell function. TCR does not contain signaling capability by itself. Instead, intracellular signaling is initiated from the signaling motif found on the cytoplasmic tails of neighboring CD3 subunits. Therefore, understanding how TCR and its neighboring CD3 subunits function as a unit is important for deciphering T cell activation and designing therapeutics aimed at shaping T-cell responses. Recently, more evidence has indicated that force is required in TCR-pMHC interaction and T cell activation, and kinetics of interaction under force show different behavior from force-free conditions. Leveraging findings from these recent studies, strong emphasis was placed on investigating the role of force in TCR triggering and signaling in this thesis.

In this thesis, two-dimensional (2D) kinetics of TCR interaction with CD3 on the extracellular domain was characterized in the present and absence of force, and the impact of mutations affecting TCR-CD3 interaction have on TCR antigen recognition was investigated. Based on these findings, TCR-CD3 interaction in the extracellular domain was identified to play a unique role of relaying force from the pMHC recognition end to the intracellar signaling end of the TCR complex.

In the second part of the thesis, the scope was extended to coreceptor CD8 and the role of force in formation of TCR-pMHC-CD8 trimolecular interaction was investigated in the context of thymocyte selection. Force was found to provide a unique readout in functional outcome of thymocytes through differentiating positive selecting ligands from negative selecting ligands. By further probing factors affecting the formation of this trimolecular interaction, the Lck-dependency in CD8 contribution to the trimolecular interaction was identified, which revealed an inside-out arm of TCR signaling to complement and influence the well-known outside-in path mediated by TCR recognition of pMHC.

Overall, these findings provide a deeper understanding of TCR triggering and early signaling from the perspective of TCR-CD3 interaction and outside-in/inside-out loop of signal integration with the common theme of mechanical force as significant factor influencing TCR function on multiple fronts.

CHAPTER 1. INTRODUCTION

T cell mediated immune response in adaptive immunity is an essential part of our defense system against bacterial and viral infections, toxins, and cancer cells. T cells generate a huge repertoire of TCRs through the rearrangement of V,D, and J gene fragments. TCRs have remarkable sensitivity as they can be triggered by as few as a single agonist pMHC. At the same time, TCRs are highly specific in the sense that they recognize specific foreign pMHCs in the presence of a large excess of self-pMHCs. In addition, small differences in the sequence of presented peptide may lead to large differences in functional outcome of T cells. Because the specific interaction between TCR and pMHC leads to T cell activation and cellular immune response, it has been the subject of extensive research aimed at figuring out how TCR triggering occurs and how is TCR-pMHC binding related to T cell signaling events. At the current state, our understanding on the mechanism of TCR triggering and its relationship to T cell signaling is still incomplete, and it is the aim of this thesis to further our understanding on this topic and contribute to the collective effort to solve the puzzle that is TCR triggering.

The objective of this thesis is to further our understanding on the role of force in T cell triggering and activation by investigating two different aspects of TCR triggering. First, emphasis was placed on probing the interaction between TCR and CD3 in the extracellular domain (Chapter 4), as it is the first point of communication between these two surface proteins and it initiates the transduction of pMHC recognition signal from TCR to intracellular signaling events occurring on the tails of CD3s. The focus of the first part is to characterize the interaction under force and force-free conditions, and relate the

kinetics of TCR-CD3 interaction to TCR antigen recognition, one of the most critical parameters in T cell mediated immune response.

In the second part of the thesis, I switched gears to expand the scope beyond the TCR complex (i.e. TCR and its neighboring CD3 subunits) to include the contribution of coreceptor CD8 in antigen recognition and cell fate in the context of thymocyte selection (Chapter5). Thymocyte selection is the process where developing T cells interaction with APCs in thymic microenvironment to coordinate a selection of functional and self-tolerant T cell repertoire. As such, this process filter out those T cells that cannot signal strongly and those that are too reactive toward self-antigens, and the unsuccessful outcome of thymocyte selection often leads to autoimmune diseases where T cells attack healthy self-tissues and cells through the recognition of self-peptides presenting on those cells. Building upon initial findings by Dr. Jinsung Hong, a past member of our lab, I found that CD8 coreceptor, with its primary functions of stabilizing TCR-pMHC interaction and delivery of Lck to the TCR complex, contribute under force to produce a unique readout relevant to the outcome of thymocyte selection. By investigating potential factors influencing the contribution of CD8 to TCR-pMHC interactions, an inside-out arm of TCR signaling was identified in the sense that the outcome of intracellular activities has a direct impact on TCR recognition of pMHC, which is the start of the outside-in signaling arm of TCR signaling.

Lastly, the thesis ends with my conclusions of current findings and recommended future directions to further what has been accomplished in this thesis and build our understanding toward solving the whole mechanism of TCR triggering (Chapter 6). A better understanding toward how T cells function is not only vital for explaining many

phenotypical symptoms we often see in T-cell mediated diseases, but also for developing better therapeutics to attenuate or strengthen T cell responses to fine tune immunity. In order to realize this end goal, there are many important questions that are still left to be addressed.

CHAPTER 2. BACKGROUND

2.1 T Lymphocytes and TCR triggering

T lymphocytes play a central role in adaptive immune response against bacteria, viruses, toxins, and cancer cells through mediating direct killing of antigen-expressing cells (1). T cells recognize antigen in the form of pMHC presented on the surface of APCs to discriminate pathogens from self-antigens. Because of the important functions of T cells, understanding the unique specificity and sensitivity of TCR have been the subject of many studies, ranging from structural studies (2) to kinetics approaches (3, 4). Utilizing kinetics-based assays, prior studies have found correlation between the affinity of TCR-pMHC interaction with T cell responsiveness (5). Despite much effort in the field to investigate how T cell ligation leads to T cell activation, the exact mechanism remains unclear. One of the key reasons for this lies in the unique structure of the TCR complex (Figure 1). The TCR complex is made of TCR with three surrounding CD3 subunits, namely CD3γε, CD3δε, and CD3ζζ (6, 7). TCR is responsible for interacting with pMHC, but it does not contain any signaling motif. Instead, intracellular signaling is initiated from the immunoreceptor tyrosine-based activation motif (ITAM) domains found on the cytoplasmic tails of CD3 subunits. Therefore, external triggering on TCR needs to be transmitted to its neighboring CD3 subunits. The transmembrane region of the TCR complex holds the different subunits together through attraction of opposite charges (8), and the presence of strong interaction has made this region a good candidate to study the communication between TCR and CD3s. However, although studies have shown that the transmembrane region could be responsible for transmitting a conformational change upon

TCR engagement (9), the earliest point of communication between TCR and CD3 remains at the extracellular domain. Despite that, specific interaction between the extracellular domains of TCR and CD3 has not been detected before using 3D kinetics measurements such as Surface Plasmon Resonance (SPR). The lack of measurement suggests that the interaction between TCR and CD3 in the extracellular domain is probably very week, if it exists. Another possible explanation for the absence of interaction can be attributed to the 'force-free' environment that the measurements were taken in. Increasing evidence has point toward the existence of force contributed by actin polymerization, actin retrograde flow and myosin II-dependent contraction during TCR-pMHC ligation formed between cell interfaces (10) and subsequent formation of immunological synapse (11, 12). In relation to TCR triggering, a recent study has highlighted the importance of force in TCR-pMHC interaction through demonstrating that force can prolong the lifetime of TCR-pMHC interaction for agonistic peptides (13), which suggests a possible mechanism of TCR using interaction duration under force as a criterion to discriminate between agonist and antagonist peptides. Given that TCR interaction with agonistic pMHC can be enhanced with force, it is reasonable to hypothesize that the communication between TCR and CD3, a crucial step required to relay the pMHC recognition signal across the membrane, occurs in the presence of force as well. This novel approach to unraveling the relationship between TCR and CD3 will be explained in more details in Chapter 4.

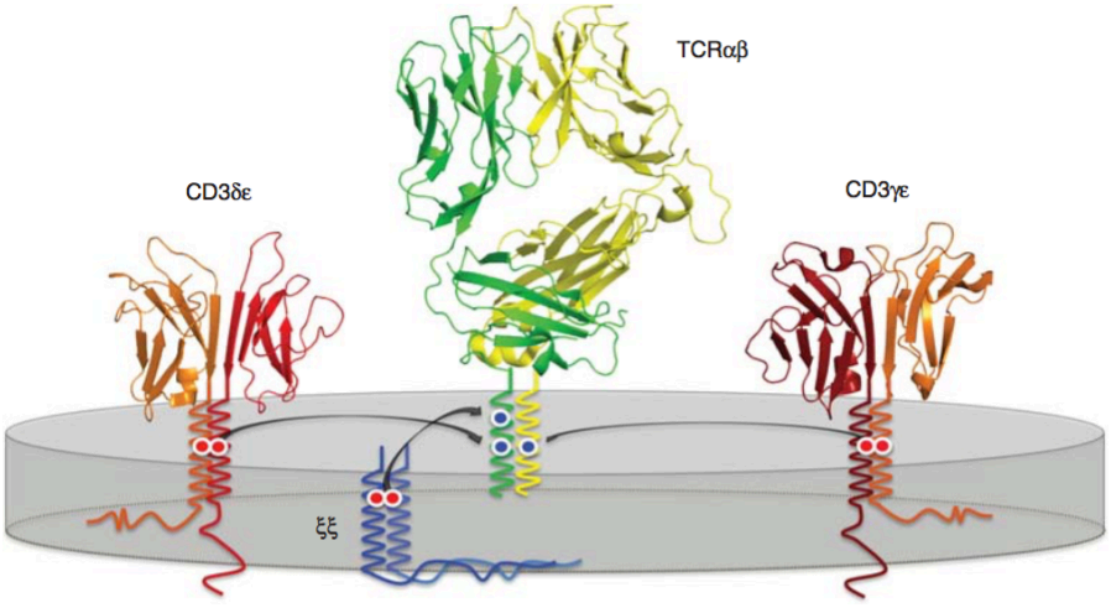

Figure 1 - Structure of the TCR complex consists of an αβTCR surrounded by three CD3 subunits, CD3γε, CD3δε, and CD3ζζ held together through attraction of opposite charges in the transmembrane region. Adapted and modified from (8).

Following TCR triggering by agonist pMHCs, the ITAMs on CD3 cytoplasmic tails will undergo phosphorylation by Lck (14). These phosphorylated ITAMs, in turn, provide docking sites for ZAP-70, another key kinase responsible for the propagation of early TCR signaling, which eventually leads to the opening of intracellular calcium channels to release Ca^{2+} from intracellular stores (15). This release of calcium flux is often used as a readout of early T cell activation (13, 16, 17). On the scale of hours, T cell activation can be characterized by expression of surface markers, and two such markers are CD69 and CD25. CD69 is one of the earliest surface antigens expressed by T cells after activation (18). Once expressed, CD69 acts as a costimulatory molecule for T cell proliferation. CD25 is the alpha chain of the Interleukin-2 (IL-2) receptor, and it is absence on naïve T cells. Following T cell activation, CD25 expression is upregulated.

2.2 T cell receptor and CD3

2.2.1 Extracellular interaction

The extracellular interaction between TCR and CD3 influences the spatial organization of the TCR complex. Prior studies have used antibody-mapping (19), structural analysis (20, 21), mutagenesis studies (22) and charge complementarity studies to identify potential mocking sites of CD3 subunits (23) (Figure 2). One prominent model of TCR-CD3 extracellular organization places CD3 heterodimers on opposite sides of the TCR (24). In particular, this model proposed, based on evidences from solved solution structures of CD3 heterodimers, that CD3γε interacts with the constant region of TCRβ, which contains the FG loop. An earlier studies used H57, a monoclonal antibody (mAB) targeting the FG loop, to demonstrate that binding of H57 to the TCR reduces the subsequent staining using mAB 2C11, which binds to CD3ε, thus highlighting the importance of the FG loop in TCR-CD3 interaction (19). Apart from these, other possible docking sites have been proposed based on analyzing the crystal structure of TCR-pMHC complexes (25). Some of these proposed docking sites are overlapping, while the rest are far apart, as shown in Figure 2. More recent, studies have used nuclear magnetic resonance (NMR) spectroscopy to identify TCR-CD3 interaction sites (26) and small-angel X-ray scattering and electron microscopy (EM) to investigate the overall organization of the TCR-CD3 complex (21). Despite that, there has not been a consensus on the exact spatial organization of the TCR complex and one of the key reasons behind that is the lack of direct evidence of TCR-CD3 extracellular interaction.

2.2.2 Signal initiation from CD3 intracellular tails

Apart from hosting the ITAMs, CD3ε cytoplasmic tails were found to show close interaction with the plasma membrane (27) using Fluorescence resonance energy transfer (FRET). This interaction involving basic residues on CD3ε and acidic phospholipids enriched in the inner leaflet of the plasma membrane embeds key tyrosines residues of ITAMs and sequesters their phosphorylation by Src kinases. A related study demonstrated that Ca^{2+} can regulate the charge property of lipids and bring about a dissociation of CD3 cytoplasmic tails from the plasma membrane (28). This new function of Ca^{2+} is thought to amplify TCR signaling through increasing the availability of ITAMs, but this phenomenon has yet to address the question of how TCR recognition of pMHC can bring about the release of CD3ε cytoplasmic tails from the membrane, since Ca^{2+} flux is a downstream signaling event and is only capable of amplifying an existing signal. The cause of this intracellular conformational change as a consequence of TCR ligation is likely transmitted across the membrane by CD3 subunits. Therefore, extensive research on the mechanism of CD3 cytoplasmic tail dissociation is warranted and should be focused not only on the intracellular conformational change alone but also its relationship to extracellular perturbation due to TCR ligation.

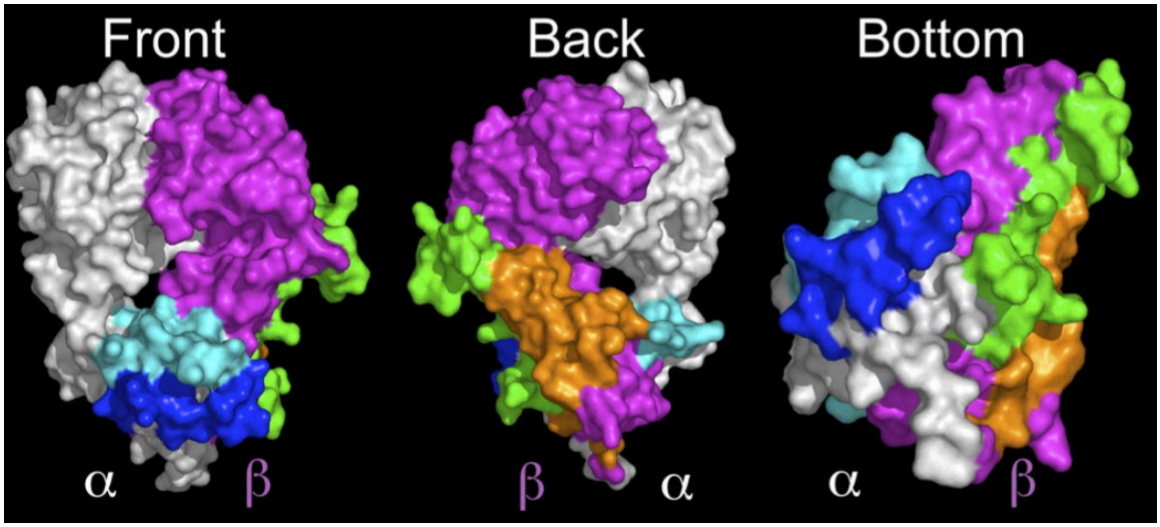

Figure 2 – TCR complex subunits and proposed extracellular CD3δε and CD3γε interaction sites with αβTCR. Different color-coding represents proposed docking sites from different studies. Adapted from (25).

2.3 Catch-bond and slip-bond

If the duration of a bond is shortened by applied force, it is typically characterized as a slip-bond. In contrast, if the duration is prolonged by applied force, it is characterized as a catch-bond. Even since the first experimental demonstration of catch-bond in the selectin system by our lab (29), many other surface receptors were found to exhibit catch-bond behavior till an optimal force level where the duration of the bond is the longest and further application of force shortens bond lifetime beyond that point (slip-bond phase). Examples of catch-bonds include TCR-pMH interaction (13), integrin α5β1 with fibronectin (30), αLβ2 with intercellular adhesion molecule-1 (31), and platelet glycoprotein Ibα interacting with von Willebrand factor (32). The collective profile of catch-then-slip bond will be referred to as catch-slip behavior in this thesis.

2.4 Thymocyte development

Committed lymphoid progenitors from bone marrow migrate to thymus via blood. Once inside the thymus, these T-cell precursors have a double negative (DN; no CD4 or CD8) phenotype (33) (Figure 3). These DN thymocytes can be further subdivided into four group based on their surface expression of CD44 and CD25, such that DN1 is $CD44^{+}CD25^{-}$, DN2 is $CD44^{+}CD25^{+}$, DN3 is $CD44^{-}CD25^{+}$, and DN4 is $CD44^{-}CD25^{-}$ (34). For cells proceeding to express αβTCR, they first express pre-Tα in association with a full TCRβ chain at the DN3 stage (35). T cells that can actively signal proceed to express full TCRα chain, and subsequently, these thymocytes start to express CD8 and CD4 coreceptors and become double-positive (DP; $CD4^{+}CD8^{+}$) thymocytes (36). The DP stage marks the onset of TCR-mediated thymocyte selection. At this stage, most of the DP thymocytes express TCRs that interact poorly with the available self-pMHC found inside the thymus that they are unable to sustain the amount of intracellular signaling required for survive, which leads to death by neglect. The other subset of DP thymocytes that interact very strongly with self-pMHC will promote rapid apoptosis as a result of their signaling response in a process called negative selection, as its purpose is to eliminate those T cells with the potential to cause autoimmune diseases if allowed to leave the thymus. The remaining subset of DP thymocytes that can maintain survival signal but do not react too strongly to self-pMHC are chosen in the process called positive selection and they proceed along its developmental pathway to become lineage specific $CD4^{+}$ or $CD8^{+}$ single-positive (SP) T cells (37).

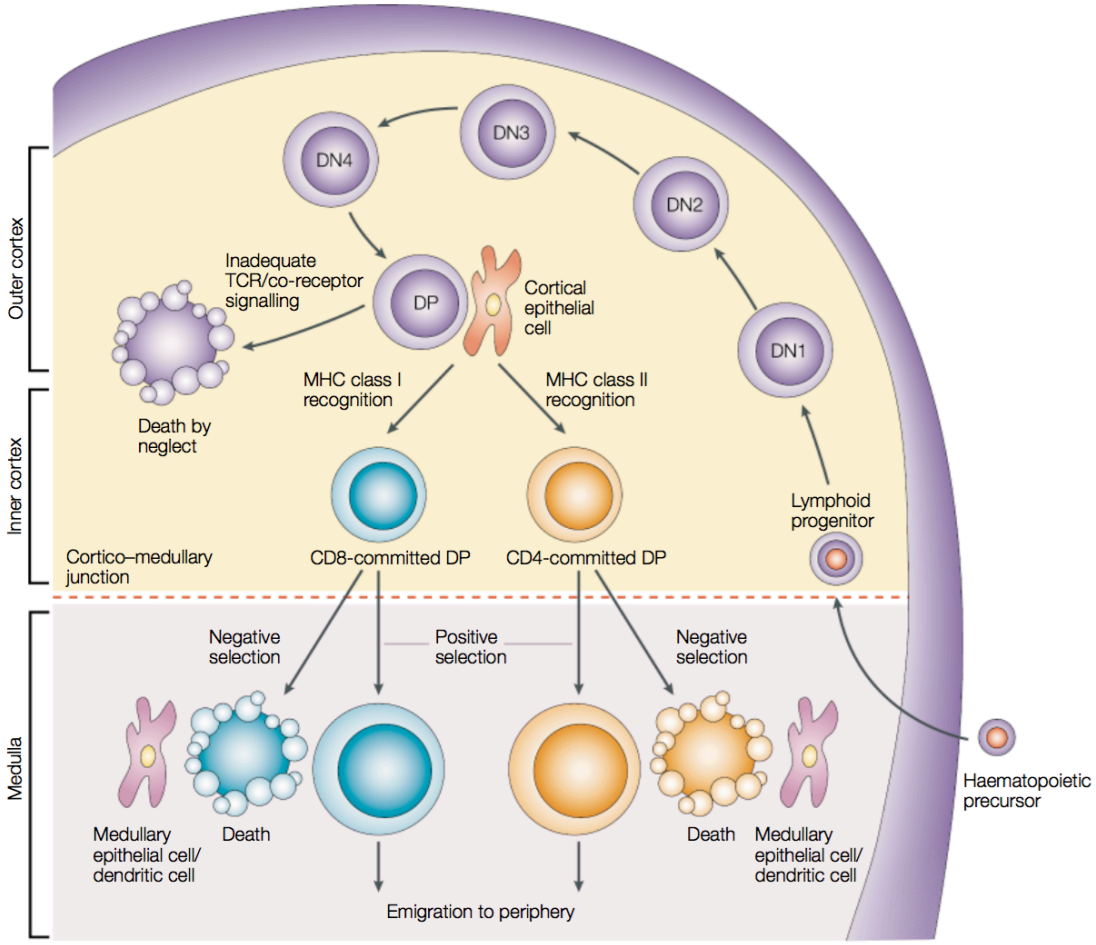

Figure 3 - Different stages of thymocyte development in the thymus. Committed lymphoid progenitor cells enter from blood and pass through DN stage to DP stage where both CD4 and CD8 coreceptors are expressed on cell surface. At the DP stage, thymocytes that do not signal are eliminated due to death by neglect. Thymocytes that interact with self-pMHC too strongly are induced to die by apoptosis. The remaining ones that signal strong enough to survive but not too strong to get negatively selected undergo positive selection and go on to lineage committed of either $CD4^+$ or $CD8^+$ SP thymocytes and prepare to migrate to periphery. Adapted and modified from (33).

2.5 CD8 co-receptor

Antigen recognition by the T cell is capable of discriminating peptides that differ by a single amino acid and trigger a wide range of T cell responses (38). TCRs bind to class I or II pMHCs with the help of CD8 or CD4 co-receptors, respectively. CD8 coreceptor

binds to α3 conservative domain of the MHC without making contact to the peptide. CD8-MHC interaction is distinct from TCR binding to MHC, which only involves the α1 and α2 domains on the MHC (39, 40). The affinity of CD8-MHC interaction is much lower than that of TCR for agonist pMHC (41), suggesting that CD8 binding to MHC is primarily a helper function to stabilize TCR-pMHC bonds, especially for low affinity targets of the TCR (42). Intracellularly, CD8 associates with Src family kinase Lck (43), and it was found that CD8 associates with CD3 in the presence of Lck (44), and the absence of CD8 prevented T Cell signaling by monomeric pMHC (45). Exactly how does pMHC bind TCR and CD8 has been a topic of much debate. Studies using soluble molecules in a fluid phase, i.e. 3D binding measurements using SPR, have generated conflicting results showing that CD8 and TCR bind pMHC independently (46), while another found that CD8 enhances TCR-pMHC interaction by reducing the off-rate (41). Utilizing 2D binding assays to better simulate pMHC interaction with TCR and/or CD8 across cell interface, a more recent study showed that CD8 binds cooperatively to TCR-pMHC interaction in a synergistic fashion to favor potent ligands by further enhancing binding and amplify discrimination of peptides (47). Building upon the findings from 2D kinetics studies and combined with the influence of mechanical force in amplifying TCR-pMHC interaction for agonist discrimination (13), I further investigated the contribution of TCR-pMHC-CD8 trimolecular interaction in the context of thymocyte selection and presented these findings in Chapter 5.

2.6 DNA-based force probes

DNA-based force probes, with easy adaptability and high uniformity, have seen increasing utilization in the study of mechano-transduction. Tension gauge tethers (TGT)

was developed to tether ligands to the substrate by a double-stranded DNA that has a defined tension tolerance for rupture (48, 49) (Figure 4A). The tension tolerance can be designed at a low (unzipping the helix), high (shearing the strands), or intermediary (combination of both) level and fine-tuned by adjusting the length and G-C contents within a force range of 12–56 pN. Rupture of the TGT by the above tolerance forces, which are generated by the cell and applied through the receptor–ligand bonds, is irreversible and it reduces the availability of the tethered ligands, thereby inhibiting force-dependent cellular functions, such as spreading, migration, or signaling. By observing cell behaviors on TGT-tagged ligands with different tension tolerances (12-56 pN), the minimum force that the cell can exert on single ligands and the threshold force required by such cell functions can be identified.

Molecular tension-based fluorescence probes use a DNA hairpin, which unfolds under force but refolds upon force removal, instead of a double-stranded DNA that ruptures irreversibly by force. The two feet of the hairpin are conjugated with a fluorophore-quencher pair, which prevents fluorescence from the fluorophore when the hairpin is folded but allows fluorescence when the hairpin is unfolded, thereby reporting the above threshold force exerted on the ligand (50-52) (Figure 4B). Since unfolding and refolding of the DNA hairpin are reversible, molecular tension-based fluorescence probes, which have a force range between 4–16 pN, can be used to visualize the spatiotemporal distributions of cell-generated tensions on the receptor–ligand bonds and can be combined with other advanced imaging techniques, such as super-resolution nanoscopy in the future to visualize force generation at a single molecule level.

More recently, the sensitivity of the DNA-based force probes are enhanced by immobilizing DNA hairpins on gold nanoparticles, allowing the fluorophore on the hairpin to be dual-quenched by both the molecular quencher and gold nanoparticle to yield ~100-fold higher signal/noise ratio due to the much lowered background (51). Ligand immobility can be overcome by anchoring probes on supported lipid bilayers with clustering controlled using a second un-quenched fluorophore (Figure 4C) (53), making these probes ideal for studying the distribution of force by specific receptors at cell-membrane interface where ligands and receptors can move laterally. Collectively, DNA-based probes are versatile tools to limit and visualize tensions on individual receptor–ligand bonds on the cell surface.

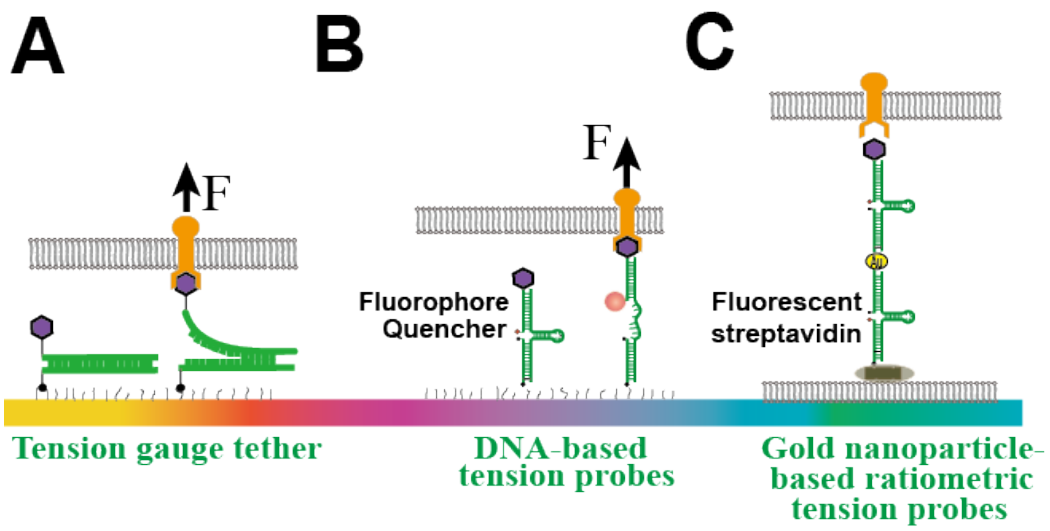

Figure 4 – DNA-based force probe designs. (**A**) Tension gauge tethers (TGT). DNA strands with defined tension tolerances are repurposed to test the tension required to activate cell adhesion. (**B**) Molecular tension-based fluorescence microscopic probe. The fluorophore and quencher are coupled to report the force-induced unfolding of the DNA hairpin, thereby unquenching the fluorescence to report molecular forces. (**C**) Gold nanoparticle-based ratiometric tension probes on supported lipid bilayer monitor hairpin opening due to force while controlling for clustering of mobile ligands using a secondary fluorescent readout.

CHAPTER 3. MATERIALS AND METHODS

3.1 Proteins, antibodies, and chemicals

3.1.1 Proteins

Mouse 2C TCR extracellular domain with a biotin-tag at its N terminus and mouse CD3γε extracellular domain with a biotin-tag at its C terminus were produced in High Five cells using baculovirus by Dr. Christopher Garcia's lab (Stanford University). The constructs for extracellular domains of CD3ε (residues 23-106, counting from the start of the leader sequence) and CD3γ (residues 23-109) included the Ig domain and conserved extracellular CxxCxE motif. To ensure proper CD3 chain pairing, the C-terminus of the CD3ε and CD3γ extracellular domains were fused to an acidic and basic GCN4 zipper (54), respectively. Each chain also contained a C-terminal hexahistidine tag for purification, while the CD3ε construct also contained a C-terminal biotin acceptor peptide (BAP) sequence for site-specific biotinylation. The constructs of extracellular domains of the 2C αβTCR (1-213 for 2C TCRα, 1-247 for 2C TCRβ, as numbered in Garcia et al 1996 (20)) containined both Ig domains in each chain and the conserved cysteine that forms an interchain disulfide bond. To ensure proper orientation relative to CD3, the BAP sequence was placed on the N terminus of the TCRα extracellular domain. Following protein expression and purification, 2C TCR and CD3εγ were each site-specifically biotinylated.

Purified proteins of human TCR, human CD3γε, human CD3δε and mouse CD3γε extracellular domains were produced by Dr. Michelle Krogsgaard's lab (New York University). 2B4 TCR constructs (both α and β subunits) contained constant domains from

human LC13 TCR with N-terminal and C-terminal biotinylation sequence. The constructs for ectodomain human CD3γε and CD3δε subunits (55, 56), wherein the two subunits are linked by a 26-residue linker, were obtained from Dr. McCluskey and Dr. Kjer-Nielson from University of Melbourne (56). The mouse CD3γε subunit construct (57), with a 26-residue linker, was obtained from Dr. Reinherz from Harvard University. N-terminal and C-terminal biotinylation sequence were added through PCR by using primers encoding the biotinylation sequence. Soluble proteins were generated by *E. coli* inclusion body expression, protein refolding and purification as previously described (58).

Recombinant pMHC monomers were from the National Institutes of Health Tetramer Core Facility at Emory University. For analysis of OTI DP thymocytes, the following peptides were synthesized and presented by mouse MHC class I H2-K^b or its mutant H2-K^bα3A2 (replacing the mouse α3 domain by that of human HLA-A2): chicken ovalbumin-derived peptide $OVA_{257-264}$ (SIINFEKL, agonist and negative selecting ligand) and its altered peptides (59) Q4 (SIIQFEKL, weak agonist and negative selecting ligand), Q4R7 (SIIQFERL, weak agonist and negative selecting ligand), T4 (SIITFEKL, weak agonist and negative selecting ligand), Q4H7 (SIIQFEHL, weak agonist and positive selecting ligand), Q7 (SIINFEQL, weak agonist and positive selecting ligand), and G4 (SIIGFEKL, weak agonist/antagonist and positive selecting ligand) as well as endogenous peptides F-actin capping protein A-derived $Cappa1_{92-99}$ (ISFKFDHL, positive selecting ligand) (60, 61) and β-catenin-derived $Catnb_{329-336}$ (RTYRYEKL, positive selecting ligand) (61). In addition, vesicular stomatitis virus-derived nucleoprotein VSV_{52-59} (RGYVYQGL) bound to H2-K^b was prepared in the same way as noncognate ligand to test CD8 binding. For the 2C TCR, SIYR (SIYRYYGL, super agonist and negative selecting

ligand), dEV8 (EQYKFYSV, agonist and positive selecting ligand), EVSV (RGYVYQEL, antagonist and positive selecting ligand), and p2Ca (LSPFPFDL, weak agonist and endogenous positive selecting ligand) peptides were bound to H2-K^b or H2-K^{bm3} (two mutations in α1 domain, Asp77Ser and Lys89Ala (62)) (63-66). All pMHC monomers were engineered to have a biotin tag on the α chain C-terminus.

3.1.2 Antibodies

Rat anti-mouse CD53 (OX-79), anti-mouce CD4-APC (RM 4-5), anti-mouse CD8a-PE (53-6.7), anti-mouse Vα 2 TCR-PE (B 20.1), anti-mouse TCRβ-PE (H57-597), anti-mouse TCRβ (H57-597), anti-mouse TCR Vβ8 (F23.1) anti-mouse Vα 11.1, 11.2 TCR-PE (RR8-1), and anti-mouse TCR Vβ8-PE (F23.1) were from BD Pharmingen. Anti-human CD3-PE (UCHT1), anti-mouse CD3ε-PE (145-2C11), anti-mouse/rat MHC II (I-E^k)-PE (14-4-4S) were from eBioscience. Anti-mouse TCRα (H28-710) was from Santa Cruz Biotechnology.

3.1.3 Chemicals

Lck inhibitor (7-Cyclopentyl-5-(4-phenoxyphenyl)-7H-pyrrolo[2,3-d]pyrimidin-4-ylamine) was from Santa Cruz Biotechnology. Anti-rat Kappa MicroBeads and MS Columns were from Miltenyi Biotech. MAL-PEG3500-SGA linker was from JenKem Technology (Beijing, China). ROCK inhibitor Y-27632 was from Sigma-Aldrich. Latrunculin A was from Abcam.

3.2 Cells

OTI and 2C TCR transgenic mice were housed at the Emory University Department of Animal Resources facility and followed protocols approved by the Institutional Animal Care and Use Committee of Emory University. CD8.4 OTI transgenic mice were gifts from Dr. Alfred Singer (National Cancer Institute). OT1 transgenic mice with 6F knock-in mutation were gifts from Dr. Paul Love (National Institute of Child Health and Human Development). Pre-selected DP thymocytes (67) were purified from a mouse thymus with $CD53^{-}$ $CD4^{+}CD8^{+}$ thymocyte enrichment by magnetic bead immunoaffinity cell sorting (MACS) according to the manufacturer's instructions (Miltenyi Biotec, San Diego, CA). In brief, thymocytes were first incubated with rat anti-mouse CD53 antibodies (BD Pharmingen) in MACS buffer (PBS without Ca^{2+} and Mg^{2+}, 2mM EDTA and 0.5% BSA) for 15 minutes at 4°C. After washing, these thymocytes were incubated with anti-rat Kappa MicroBeads (Biotech) in MACS buffer for 15 minutes at 4°C. Following another washing step, these thymocytes were resuspended in 500 ul of MACS buffer and added to MS Column. CD53- cells that passed through the MS Column (Miltenyi Biotec) were collected for experimental uses. Since CD53 expression and positive selection strongly correlated, it was selected as a purification marker (68).

17αβ OT1 hybridoma and OT1 hybridoma with CxCP mutation were gifts from Dr. Nicholas Gascogine (National University of Singapore). Mouse 58-/- T cell hybridoma transfected with mutant 2B4 TCR constructs through retroviral transduction were gifts from Dr. Michelle Krogsgaard (New York University).

3.3 Flow cytometry

Samples were incubated in 100 ul of FACS buffer (PBS without Ca^{2+}, Mg^{2+}, 5 mM EDTA, 2% FBS) containing 10 ug/ml of antibodies of interest to stain for 30 min in 4°C. Samples were then washed twice with 200 ul of FACS buffer and resuspended in 350 ul of FACS buffer for analysis using LSR II flow cytometry (BD Biosciences). Flow cytometric data were analyzed using FlowJo (TreeStar).

3.4 2D kinetics assays

3.4.1 Micropipette adhesion frequency assay

The theoretical framework and detailed experimental procedures have been described previous (5, 69). To summarize, binding events of red blodd cells (RBCs) coated with controled density of the protein of interest or cell expressing the protein of interest were measured against another RBC coated with controled density of the interacting partner of the protein of interest at various contact times. Human RBCs from healthy donors were first biotinylated using different concentrations of biotin to vary the maximum level of surface proteins that can be coupled on each RBC. In the example of TCR-CD3 interaction, after functionalizing these RBCs through incubation with saturating amount of streptavidin (SA) and washing, purified and biotin-labeled TCR and CD3 molecules were coated onto RBCs through biotin-SA coupling in a 30-minute incubation step followed by washing steps to eliminate uncoated proteins.

Surface densities of 2C TCR and CD3 molecules on the RBCs were quantified by flow cytometry using PE-labeled anti-mouse TCR Vβ8 (Clone F23.1, BD Pharmingen) and PE-labeled anti-mouse CD3ε (Clone 145-2C11, eBioscience), respectively. Surface densities of 2B4/LC3 TCR with human constant region and human CD3 molecules were

measured using PE Rat anti-mouse Vα11.1, 11.2 TCR (Clone RR8-1, BD Pharmingen) and PE anti-human CD3ε (Clone UCHT1, eBioscience), respectively.

In the example of TCR-CD3 interaction, two individual RBCs coated with TCR and CD3 molecules, respectively were aspirated by two apposing micropipettes and maneuvered by micromanipulation to precisely set up cell-cell contact with defined contact area and contact time and the presence or absence of adhesion events were detected by using RBC as an ultrasensitive force sensor (70) and denoted as 1 for adhesion and 0 for no adhesion over 50 contact cycle for each cell pair (Figure 5). The resultant adhesion frequency curve (P_a vs t_c) shows a monotonic increase of adhesion frequency with increasing contact time then reaches a plateau. The shape of the curve can be fitted using a probabilistic kinetics model with the following equation assuming a single step first order reaction

$$P_a = 1 - \exp\left(-m_r m_l A_c K_a [1 - \exp\left(-k_{off} t_c\right)\right] \quad (1)$$

where P_a is the adhesion frequency, m_r and m_l are the respective surface densities of the protein of interest and its interacting partner on the RBCs. A_c is the contact area, K_a is the 2D affinity in (um^2), and k_{off} is the off-rate (s^{-1}). Since A_c and K_a cannot be separated from the curve fitting, they are lumped together as the effective 2D affinity, A_cK_a.

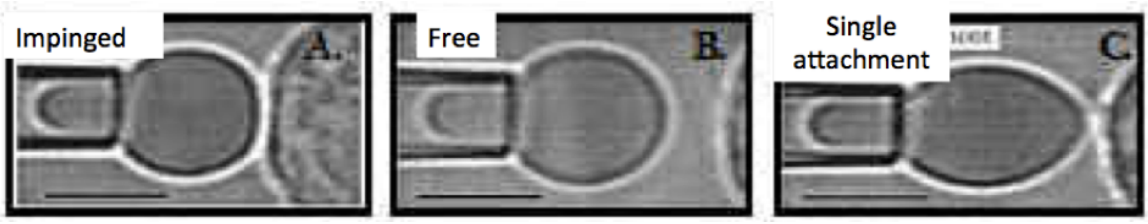

Figure 5 – Sample images showing cell-to-cell contact in micropipette adhesion frequency assay. (**A**) impinged cell contact, (**B**) a sample event showing the absence of adhesion, and (**C**) an event with adhesion.

3.4.2 Biomembrane Force Probe force-clamp assay

Detailed experimental procedures of a BFP force-clamp assay has been described previously (71). Briefly, BFP force-clamp assay measures single bond lifetime of interacting proteins in response to force. Biotinylated proteins were coated onto SA-conjugated glass beads. Using the example of TCR-CD3 interaction, a probe bead (Figure 6A) coated with TCR proteins was attached to a human RBC functionalized with biotin, which acted as an ultrasensitive force sensor with known spring constant preset to 0.3 pN/nm (71). Similar to the micropipette adhesion frequency assay, the RBC and a target bead coated with CD3γε or CD3δε were aspirated by two apposing micropipettes and brought to approach, impinge, and contact for a defined duration before the target bead was retracted (Figure 6B). Through tracking the edge between the glass bead and the RBC using a high-speed camera at 1000 fps, the magnitude of force sustained in the interaction was determined to picoNewton precision. In a force clamp experiment, the retraction of the bead was stopped once the interaction sustained a desired amount of force, and the force was sustained until bond rupture, with the total duration defining the lifetime of the interaction at that force level. Multiple measurement cycles generated bond lifetimes at

various force levels, and the results were plotted as average bond lifetime vs average force by binning of events based on force.

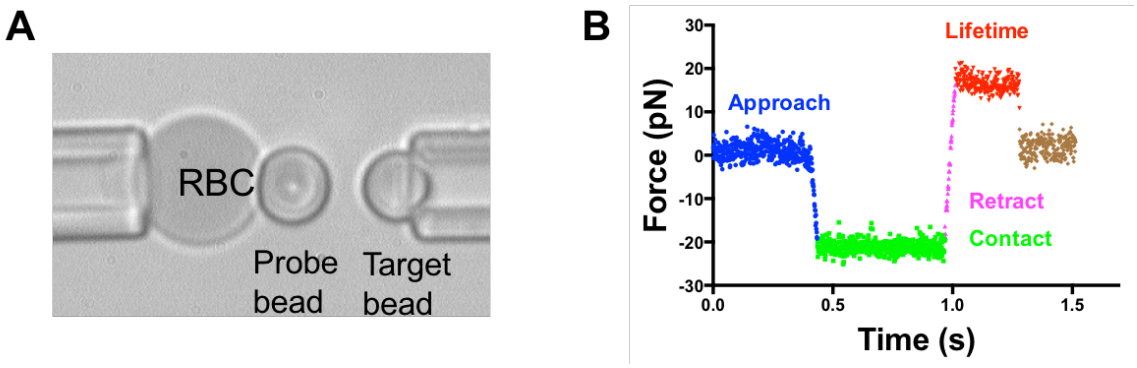

Figure 6 – Force-clamp assay using biomembrane force probe. (**A**) Schematics of the BFP setup showing a biotinylated RBC aspirated by a micropipette. A probe bead (left) was placed on the apex of the RBC through biotin-SA interaction. A target bead (right) was aspirated by a second micropipette and aligned against the center of the probe bead to establish contact driven by piezoelectric translator. (**B**) Representative force trace during a measurement cycle where a lifetime event was detected at the set force level.

3.4.3 BFP thermal fluctuation assay

Thermal fluctuation mode was used to measure lifetime of protein-protein interaction in the absence of force (72). In this mode, the target bead (Figure 6A) was retracted till the impinging force was no longer present and the protein pairs were allowed to interact through thermal fluctuation. The association and dissociation of protein-protein interactions were identified from the reduction and resumption, respectively, of thermal fluctuation. Lifetime was measured as the duration from fluctuation reduction to resumption indicated by the analysis of standard deviation of the bead movement. Modeling the kinetic process as a single-step first-order dissociation of a single monomeric bond, the probability P_b of a bond formed at time 0 to remain intact at time t_b is given by the equation

$$P_b = \exp(-k_{off} t_b). \quad (2)$$

Taking a natural log to linearize the exponential component of the equation, the resultant ln(# of events with a lifetime ≥ t_b) vs t_b plot was fitted by a straight line with the negative slope of the fitted line representing an estimate of the off-rate k_{off} (29).

3.5 Molecular stiffness analysis

A detailed description of method to measure molecular stiffness was described previously (73). In brief, the slope of force vs. displacement curve obtained during the ramp phase of BFP measurements is the stiffness of the system, which is consisted of the stiffness of the cell and that of the molecular complex in series. As such, the reciprocal of the system stiffness, $1/_{k_{mol\text{-}cell}}$, equals the sum of the reciprocals of the cellular and molecular stiffness, $1/k_{cell} + 1/k_{mol}$. Based on the assumptions of 1) molecular complex can resist tension but not compression, and 2) cellular spring has the same stiffness regardless of whether the cell surface is pulled or pushed, k_{cell} and $_{k_{mol\text{-}cell}}$ can be estimated from the respective slopes of force vs. displacement curve for compression and tension. The molecular stiffness was calculated using the equation $k_{mol} = 1/(1/_{k_{mol\text{-}cell}} - 1/k_{cell})$.

3.6 DNA force probe

All oligonucleotides were custom synthesized and purified by Integrated DNA Technologies. The design of the probe consisted of a ssDNA hairpin hybridized through two 21-mer DNA handles to the ligand and anchor strands. The 3' terminus of the anchor strand was modified with an amine group (NH_2) to immobilize the oligonucleotides on a functionalized surface, while the 5' terminus of the ligand strand was modified with a biotin

group for ligand attachment through biotin-streptavidin interaction. Two different designs of DNA force probes were calibrated by BFP to measure $F_{1/2}$ (the force at which 50% of hairpins unfold) of each hairpin and they were found to be 4.7 pN and 13.1 pN (Figure 7). These DNA force probes were functionalized on to MPTMS-treated glass surfaces using MAL-PEG3500-SGA linker (JenKem Technology) then linked to pMHC using biotin-streptavidin interaction. Anti-mouse CD11a (LFA-1) antibodies were incubated together with the DNA force probes in a 1:10 ratio to facilitate anchoring of thymocytes on the glass surface. These anti-LFA-1 antibodies were not conjugated to DNA force probes and did not contribute to fluorescence signal. OTI thymocytes were injected onto the coverslips and allowed to settle for 5 minutes before imaging using a Zeiss LSM 710 confocal microscope at room temperature for maximum of 30 minutes. During these 30 minutes, either single snapshot of multiple spots containing thymocytes interacting with the functionalized surface or time lapse imaging of single cells for 9 minutes were performed. During Lck inhibition treatment, cells were allowed to settle onto the coverslip containing 4 uM of Lck inhibitor for 5 minutes before imaging experiments in the presence of the inhibitor were performed. For other drug treatment experiments, the conditions were 20 minutes of time lapse image with 5 minutes of imaging intervals on multi-position imaging module. Upon unfolding of the DNA hairpin, an increase in Cy5 emission intensity was detected due to the separation between the fluorophore and the quencher on the DNA force probe. Image analyses were performed using ImageJ.

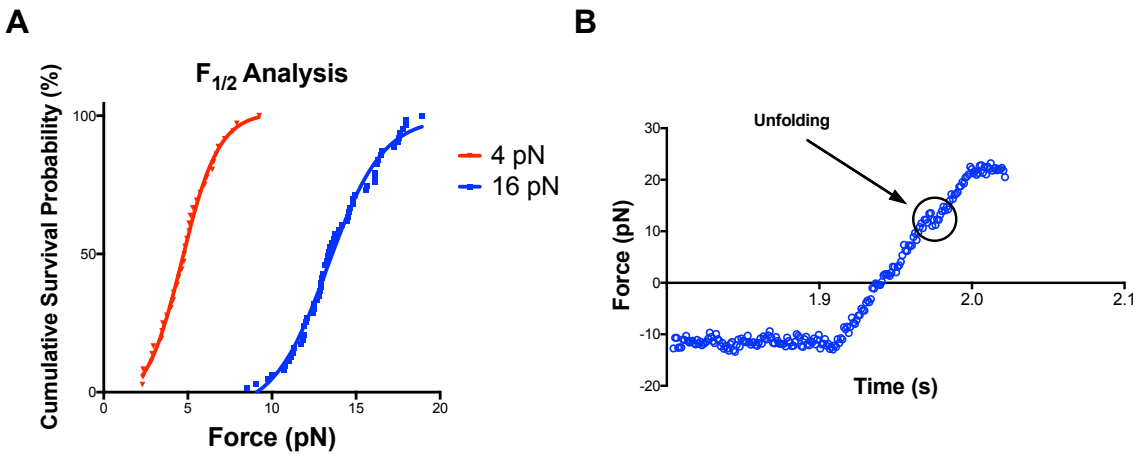

Figure 7 - Calibration of DNA force probes. (**A**) Opening force $F_{1/2}$ of 4 pN and 16 pN force probes measured by BFP. The values were determined at the point where half of the probes are open. (**B**) Representative unfolding event showing a drop of force level during the ramping phase of BFP. The dip in force level corresponded to a lengthening of construct under force as the DNA hairpin unfolded.

3.7 Statistical analysis

F-test was used in spring constant analysis to assess the goodness of fit of Gaussian distribution on a population of molecular spring constant values. Linear regression was performed on thermal fluctuation data sets to generate lines of best fit for the estimation of 2D off-rates. Comparison between two groups of data were done using student's t-test. One-way ANOVA was used for comparison between multiple groups of data. Data were represented as mean ± SEM unless otherwise stated.

For force vs. lifetime data generated by BFP assay, catch-slip bonds were fitted with a single Gaussian distribution and different catch-slip bonds were compared against each other using a null hypothesis that one curve was needed for both data sets, and an alternative hypothesis that different curve was needed for both data sets. The null hypothesis was rejected when p was found to be less than 0.05 using F-test.

CHAPTER 4. KINETIC CHARACTERIZATION OF SPECIFIC INTERACTION BETWEEN TCR AND CD3 IN THE EXTRACELLULAR DOMAIN

4.1 Introduction

T lymphocytes play a central role in adaptive immune response against bacteria, viruses, toxins, and cancer cells (74). T cells recognize antigen in the form of peptide (p) presented on the major histocompatibility complex (MHC) expressed on the surface of APCs to discriminate pathogens from self-antigens (74, 75). Prior studies have indicated the affinity of TCR-pMHC interaction correlates with T cell responsiveness (3-5). Despite much effort in the field to investigate how T cell ligation leads to T cell activation, the exact mechanism is still poorly understood. One of the key reasons for this lies in the unique structure of the T-cell receptor (TCR) complex. While pMHC is bound to the membrane distal domains of the α and β subunits of TCR, intracellular signaling events are mediated by CD3 dimers (CD3ζζ homodimer, CD3γε heterodimer, and CD3δε heterodimer) that contain at least one conserved immunoreceptor tyrosine-based activation motif (ITAM) (8, 14, 76). As such, signaling initiation from pMHC engagement of the TCR has to be transmitted to CD3 through specific interactions between TCR and CD3. However, direct binding measurement of specific interaction between the extracellular domains of TCR and CD3 by 3D kinetics measurements such as Surface Plasmon Resonance (SPR) was not possible due to the estimated low affinity of this interaction (24, 57) and other methods, such as the ones utilizing mutagenesis, were only able to elicit indirect results of this particular interaction (22). Recent studies have used nuclear

magnetic resonance (NMR) spectroscopy to identify TCR-CD3 interactions sites (26, 77) and small-angle X-ray scattering and EM to investiage the overall organization of the TCR-CD3 complex (21). However, none of these studies were able to quantify and characterize the interaction amongst the different subunits of the TCR complex, which is critical for unraveling the triggering mechanism of TCR and its subsequent signal transduction during T cell activation. Mapping out the specific interactions amongst different components of the TCR complex not only serves to furhter our understanding on how T cell triggering relates to activation, but also plays an essential role in directing efforts toward discovering potential therapeutic targets capable of modulating T cell responses.

The interplay between TCR and CD3 has been a topic of great interests over the last two decades. Cystal structure of TCR extracellular domain (20) and solution and crystal structures of the extracellular domain of CD3δ, γ, and ε (24, 56, 57, 78) provided an excellent starting point in unraveling the structural basis of the TCR complex and the organization of its various components. Dimerization of TCR or clustering of TCR has been suggested as a key step in TCR signaling based on TCR or CD3 cross-linking studies (79-82). Another model on T-cell signaling involes conformational change of the TCR-CD3 complex subunits with respect to each other and/or the membrane (25, 83). In relation to the conformational change model, a new line of studies that focus on the role of mechanical force in T cell activation have emerged on the field. The central hypothesis of these studies is that TCR-pMHC interactions formed across cell interface are likely subjected to mechanical forces (84-86) and the TCR-CD3 subunits move as a unit to undergo conformational change under the influence of mechanical force. In the ‘mechanosensor’ model, it was proposed that TCR-pMHC interaction is capable of

generating a torque, resulting in the FG loop of TCR to act as a lever pressing on the extracellular domain of CD3ε, which is thought to stiffen and transfer force through the membrane to generate downstream signaling (16, 57, 87). More recently, one study has demonstrated that force can prolong the lifetime of TCR-pMHC interaction for agonistic peptides (13), while another showed that T cell ligation may lead to actin polymerization and generation of protrusive forces (12). Theses studies highlighted the relevance and importance of force as a potential regulator of T cell response. It seems reasonable to hypothesize that since mechanical force influences TCR-pMHC interaction at the site of triggering, the immediate next link, TCR-CD3 interaction, is likely subjected to force upon antigen engagment and the ability of CD3 to transfer force signal from TCR plays a key role in signal initiation of the TCR complex.

In this study, I measured the 2D kinetics (69) of the specific interactions between the extracellular domains of mouse and human TCR and CD3 *in vitro*, and used Biomembrane Force Probe (BFP) (71) to investigate TCR-CD3 interaction under force. Measurements of specific interactions between TCR and CD3 ectodomains allowed us to provide insight on the arrangement of the members within the TCR complex and the molecular mechanism for dimerization of TCR-CD3. Theses findings on the enhancement of TCR-CD3 interaction under force strengthened the role of CD3 as a force transducer and redefine the model of TCR early triggering by providng a more complete picture on howTCR-pMHC recognition signal gets converted to intracellular signaling.

4.2 Results

4.2.1 Characterization of 2D kinetics of mouse TCR-CD3 extracellular domains revealed specific interaction

To address the gap of knowledge revolving around the presence of specific interaction between TCR and CD3 in the extracellular domains, I first tried to determine whether the extracellular domain of mouse 2C TCR and CD3γε interact by assessing the 2D kinetics of these two proteins using the micropipette adhesion frequency assay. Since TCR and CD3γε interact through cis-interactions on a single cell membrane under physiological conditions, I tried to simulate this orientation to my best capabilities by orientating the 2C TCRs via its N-terminus and CD3γε via its C-terminus on separate RBCs (Figure 8A). As such, when the two RBCs were brought into contact, TCR and CD3γε assumed a "pseudo-cis" orientation similar to the physiological conditions. Non-specific interactions were controlled through measuring the adhesion frequency between the protein of interest (2C TCR or CD3γε) with streptavidin-coated RBCs, and negligible level of adhesion was detected for both cases (Figure 8B).

As shown in Figure 8C, the effective 2D affinity between mouse 2C TCR and mouse CD3γε was determined to be 3.4×10^{-5} um^4. At the same time, specific homotypic interaction of CD3γε was also measured using CD3γε orientated through its N-terminus on one RBC and through its C-terminus on the other RBC. The effective 2D affinity of CD3γε homotypic interaction was determined to be 2.3×10^{-5} um^4. The off-rates of these interactions were measured by thermal fluctuations assay to be 12.8 s^{-1} for TCR-CD3γε and 8.3 s^{-1} for CD3γε homotypic interaction. Adhesion frequencies at various contact times

were measured for the 2C TCR-CD3γε interaction (Figure 8D) and CD3γε homotypic interaction (Figure 8E), while non-specific interaction is shown in black in the same graph.

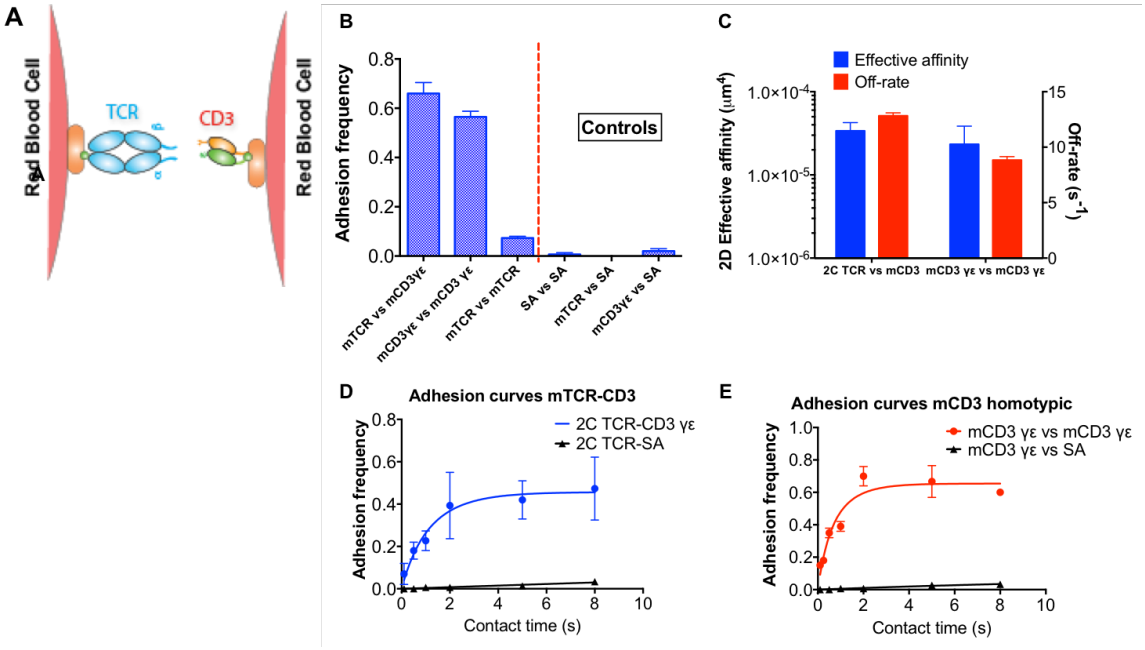

Figure 8 – 2D kinetics of mouse TCR-CD3 interaction. (**A**) Micropipette setup showing orientation of purified TCR and CD3. (**B**) direct comparison of adhesion frequency between mouse 2C TCR and mouse CD3γε, mouse CD3γε homtotypic interaction, mouse 2C TCR homotypic interaction versus that of the non-specific controls (streptavidin-coated RBCs versus itself and the proteins of interests). (**C**) Summary of 2D effective affinity and off-rate of mouse 2C TCR-CD3γε interaction and mouse CD3γε homotypic interaction. (**D**) Mouse 2C TCR-CD3γε adhesion curve, and (**E**) mouse CD3γε-CD3γε adhesion curve.

Adopting a similar "pseudo-cis" orientation, the interaction between extracellular domain of 2B4 TCR expressed with human constant region and human CD3γε and CD3δε were assessed using the micropipette assay, and specific interactions were detected (Figure 9A). The 2D effective affinity between human TCR constant and human CD3γε was $3.4x10^{-6}$ um^4 and that for CD3δε was $2.1x10^{-6}$ um^4. Interplay between human CD3 dimers was investigated and specific interactions were measured for each of the different combinations. CD3γε-CD3δε heterotypic interaction had the highest 2D effective affinity

($1.1x10^{-5}$ um^4) amongst heterotypic interactions. In terms of homotypic interactions, 2D effective affinity was $6.6x10^{-6}$ um^4 for CD3γε and $2.0x10^{-4}$ um^4 for CD3δε, and $2.6x10^{-6}$ um^4 for TCR.

Off-rates of TCR-CD3γε and TCR-CD3δε were measured by thermal fluctuation assay to be 14.1 s^{-1} and 11.1 s^{-1}, respectively (Figure 9B). Off-rate of CD3γε–CD3δε heterotypic interaction was found to be 14.9 s^{-1}.

It is worth noting that crosstalk between human CD3 and mouse TCR was not observed, as no adhesion event was detected between these two proteins.

These observations (Table 1) strongly suggest the presence of a specific binding site between the extracellular domains of TCR and CD3γε subunits. Furthermore, the homotypic and heterotypic interactions observed between CD3 subunits could play a relevant role in the formation of multimers of TCR-CD3 complex as the presence of extracellular interactions can potentially provide stabilizing effect to dimeric TCR-CD3 complex.

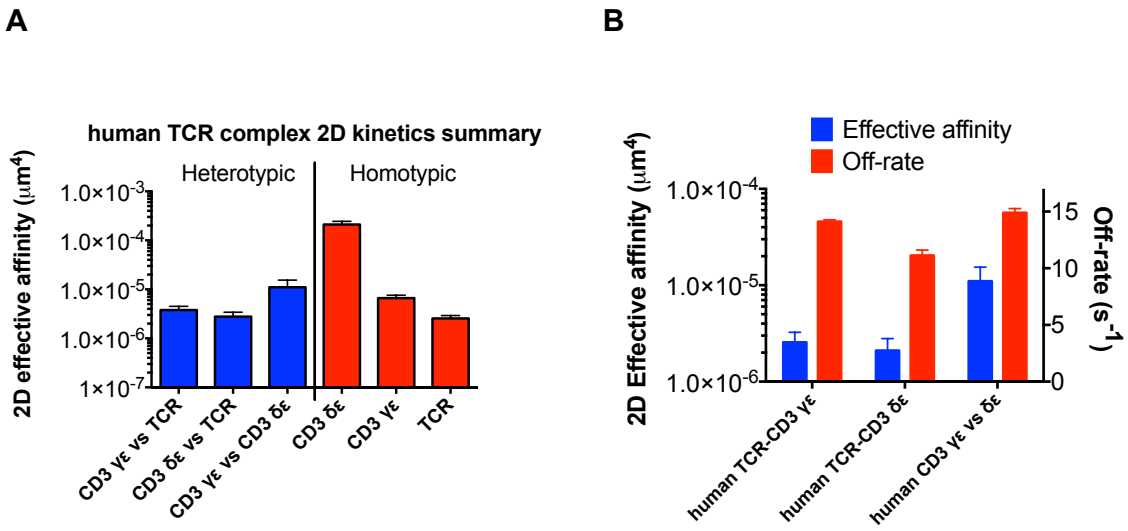

Figure 9 - 2D affinity of human TCR-CD3 extracellular interactions. (**A**) 2D affinity of heterotypic and homotypic extracellular interactions amongst members of the human TCR complex. (**B**) Comparison of 2D effective affinity and off-rate of human TCR-CD3γε, human TCR-CD3δε, and CD3γε-CD3δε interactions. Data are mean ± SEM.

Table 1 - Summary of 2D kinetics of TCR-CD3 interactions

	2D $AcKa$ (um^4)	2D k_{off} (s^{-1})	2D A_cK_{on} (um^4s^{-1})
2C TCR vs mCD3γε	$3.38 \pm 0.87 \times 10^{-5}$	12.8 ± 0.28	$4.33 \pm 1.12 \times 10^{-4}$
mCD3γε vs mCD3γε	$2.33 \pm 1.53 \times 10^{-5}$	8.83 ± 0.32	$2.06 \pm 1.35 \times 10^{-4}$
hTCR vs hCD3γε	$2.56 \pm 0.69 \times 10^{-6}$	14.1 ± 0.15	$3.62 \pm 0.98 \times 10^{-5}$
hTCR vs hCD3δε	$2.10 \pm 0.70 \times 10^{-6}$	11.1 ± 0.48	$2.34 \pm 0.79 \times 10^{-5}$
hCD3δε vs hCD3δε	$1.10 \pm 0.44 \times 10^{-6}$	14.9 ± 0.37	$1.64 \pm 0.66 \times 10^{-5}$

4.2.2 FG loop has a major contribution to TCR-CD3 extracellular interaction

The FG loop on TCRβ constant region has been implicated as one of the key sites of interaction between TCR and CD3 in various studies (16, 19). Therefore, I blocked this interaction by H57-597, which is an antibody targeting the FG loop on the murine TCRβ (19). In the presence of H57-597, the adhesion frequency between 2C TCR and CD3γε dropped significantly from 37% to 6% (Figure 10A), thus confirming the importance of the FG loop in mediating specific interactions between TCR-CD3 extracellular domain. Similarly, the 2C11 antibody that binds to mouse CD3ε reduced the adhesion frequency from 59% to 8% when present during the assay (Figure 10B). However, it is worth noting that the level of adhesion did not get abolished completely in the presence of either antibody, indicating that there might be other sites of interaction between TCR and CD3γε distinct from the FG loop, such as the Cα DE loop and Cβ CC' loops (6). As a negative control, F23.1 antibody targeting the variable region of TCRβ did not cause a significant drop of adhesion frequency after blocking (Figure 10C), suggesting that the presence of antibody alone does not lead to reduction in binding. Blocking with H28-710 antibody, which binds to the constant region of mouse TCRα (88), also did not lead to a drop in adhesion frequency (Figure 10D). The results so far strongly suggest that the region targeted by H57-597, which includes the FG loop, is a major contributor to the TCR-CD3γε interaction observed.

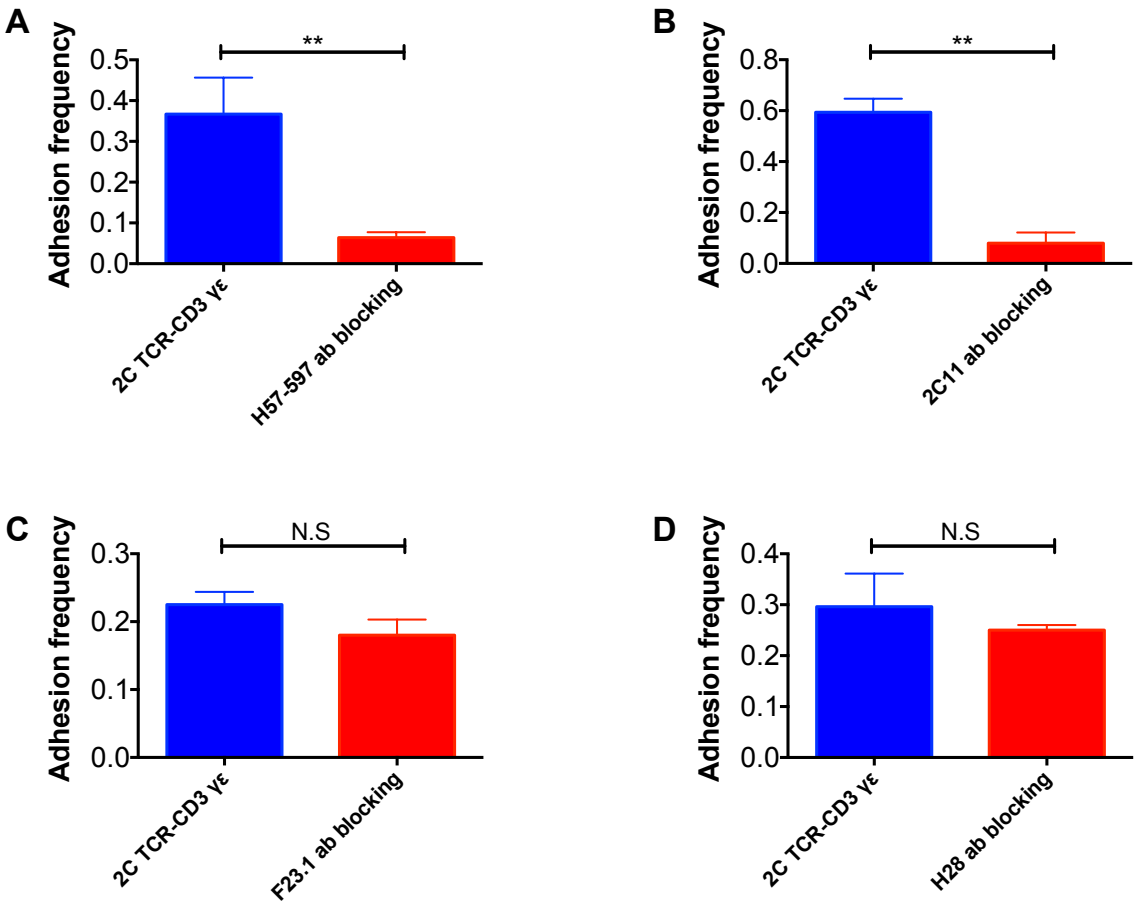

Figure 10 – The effect of antibody blocking on the adhesion frequency between mouse 2C TCR-CD3γε interaction. (**A**) H57-597 antibody blocking and (**B**) 2C11 antibody blocking resulted in a significant decrease in adhesion frequency, $p < 0.05$. (**C**) F23.1 antibody blocking and (**D**) H28-710 antibody blocking did not lead to a significant decrease in adhesion frequency. Results were analyzed by student's t test. Data are mean ± SEM.

4.2.3 TCR-CD3 interaction exhibits a catch-slip behavior under force

A recent study from the Zhu lab demonstrated a role for mechanical force on TCR-pMHC interaction and found that TCR interaction with agonist pMHCs can be prolonged under force till a peak force level around 10 pN (13). As a bridge between TCR-pMHC recognition and initiation of intracellular signaling, CD3 is likely subjected to force as a result of TCR-pMHC engagement, and I tested this hypothesis by investigating the

contribution of mechanical force in mediating TCR-CD3 interaction. A biomembrane force probe (BFP) assay was used to measure the lifetime of interaction between 2C TCR and CD3γε at various clamp forces (Figure 11A, B), and the resultant lifetime vs. force curve displayed a catch-slip behavior (Figure 11C). As the clamping force between TCR and CD3 increased from 0 pN to 10 pN, the lifetime of TCR-CD3γε interaction increased with increasing force, and this characteristic is typically called the 'catch-bond'. The peak lifetime occurred at around 10 pN, and beyond this force level, lifetime of interaction decreased with increasing force, and this characteristic is termed 'slip-bond'. CD3γε homotypic interaction also displayed a catch-slip behavior, albeit much less pronounced than TCR-CD3γε interaction (Figure 11C). In comparison, the force at which peak lifetime occurred for TCR-CD3γε interaction coincided with that of the interaction between naïve 2C TCR and agonist pMHC SIYR (Figure 11C). This finding suggests that the force experienced by TCR-pMHC is likely transferred to TCR-CD3 interaction, as both interactions are enhanced to their maximal values (longest bond lifetime) at very similar force range (~ 10 pN).

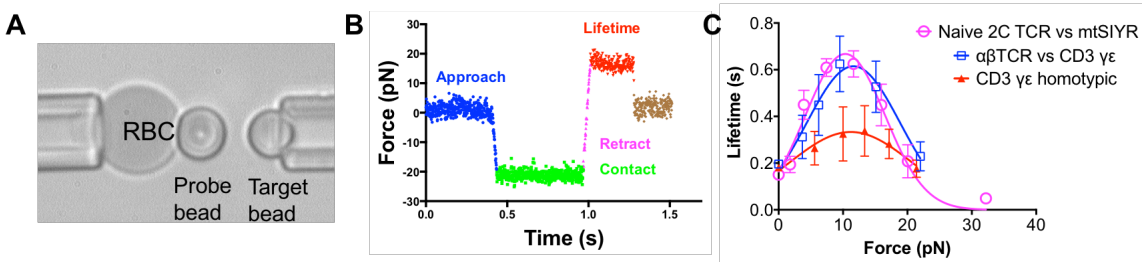

Figure 11 – Mouse TCR-CD3 interaction exhibits 'catch-slip' behavior under force. (**A**) Schematics of the BFP setup showing a biotinylated RBC aspirated by a micropipette. A probe bead (left) was placed on the apex of the RBC through biotin-SA interaction. A target bead (right) was aspirated by a second micropipette and aligned against the center of the probe bead to establish contact driven by piezoelectric translator. (**B**) Representative force trace during a measurement cycle where a lifetime event was detected at the set force

level. (**C**) Lifetime versus force curves showing that mouse 2C TCR-CD3γε extracellular interaction exhibits 'catch-slip' behavior (blue) with a peak lifetime occurring at approximately 10 pN, which coincide with that between naïve 2C TCR versus SIYR pMHC (pink, adapted from (13)). CD3γε homotypic interaction displayed a less pronounced catch slip behavior (red). Curves were fitted with Gaussian distribution, and significant differences were found between TCR vs CD3 and CD3γε homotypic interaction curves and between 2C TCR vs SIYR and CD3γε homotypic interaction curves ($p < 0.05$). Data are mean ± SEM.

Similar to mouse TCR-CD3γε interaction, human TCR-CD3 interactions displayed catch-slip behavior for both TCR-CD3γε and TCR-CD3δε (Figure 12). The force at which peak lifetime occurred was ~15 pN for both CD3δε and CD3γε. Lifetime was increased to seven times its zero-force value for TCR-CD3δε and five times its zero-force value for TCR-CD3γε at their peaks. CD3 heterotypic interaction showed a less pronounced catch-slip behavior with significantly lower lifetime at various force levels compared with TCR-CD3 interactions. The findings from human TCR-CD3 interactions corroborate well with that from the murine system to highlight the significance of force in modulating TCR-CD3 extracellular interaction.

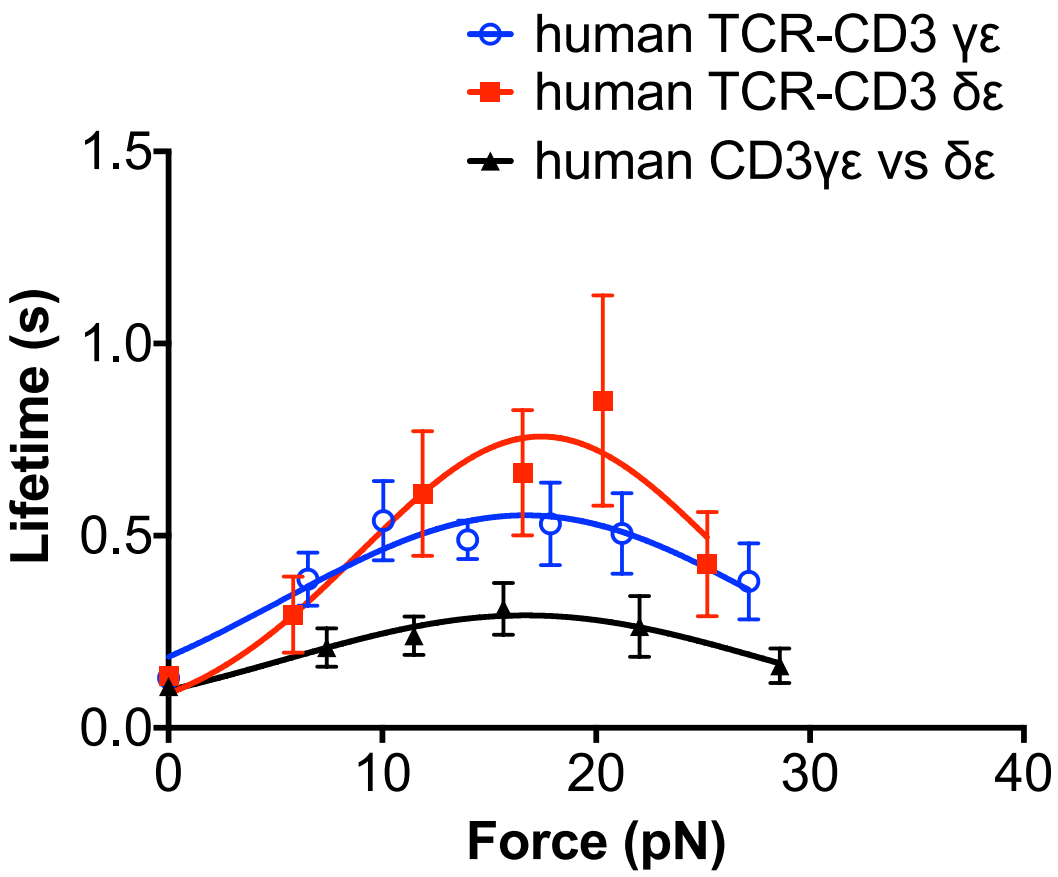

Figure 12 - Human TCR-CD3 extracellular interactions under force exhibit 'catch-slip' behavior for TCR-CD3γε (blue), TCR-CD3δε (red), and CD3γε-CD3δε (black). Curves were fitted with Gaussian distribution, and significant differences were found between TCR vs CD3γε and CD3γε-CD3δε heterotypic interaction curves and between TCR vs CD3δε and CD3γε-CD3δε heterotypic interaction curves ($p < 0.05$). Data are mean ± SEM.

4.2.4 Mutations affecting TCR-CD3 extracelluar interaction can impact TCR-pMHC recognition

Previous NMR studies (26) identified potential interaction sites for CD3γε and CD3δε on the 2B4 TCR constant region and when specific mutations were introduced in these sites and expressed in T cells, they caused a decrease in T cell function upon activation with pMHC indicating that the identified interaction sites were functionally

relevant. To determine and quantify the effect of these specific mutations on binding affinity of the extracellular interaction between mutant TCR and CD3γε, I measured the kinetics of the interaction between CD3 subunits and the WT TCR and mutants (N205AH206A, N180AQ191A, and Q138AK139A) (26) using the micropipette adhesion frequency assay. Interestingly, I observed comparable 2D effective affinity in the presence or absence of these point mutations (Figure 13A). However, when I measured the lifetime of these interactions at various forces, the results showed a catch-slip behavior for TCR NH-CD3γε and a less pronounced catch-slip behavior for TCR E133AI134A (EI)-CD3γε (Figure 13B). In comparison with wildtype (WT) TCR, these mutant TCRs showed a lower peak lifetime occurring at a lower force (Figure 13B). TCR EI, which showed the lowest IL-2 production (26), had the lowest magnitude of lifetime at peak level. The correlation between the weakening of TCR-CD3 extracellular interaction under force for mutant TCRs and the reduction in functional outcome from cells expressing these mutant TCRs strongly suggests that TCR-CD3 extracellular interaction serves as a link from TCR-pMHC recognition signal to intracellular signaling response, and a disruption of TCR-CD3 extracellular interaction is likely going to impact intracellular signaling adversely.

To strengthen my hypothesis that TCR-CD3 extracellular interaction plays a key role in relaying signaling from pMHC recognition to T-cell signaling initiation, I tested the impact of TCR mutations on pMHC recognition using hybridoma cells expressing these TCR mutants. Adhesion frequency vs contact time curve was measured for WT TCR to establish the contact time required for the interaction to reach a plateau (i.e. no further increase in adhesion frequency with increasing contact time) (Figure 14A). As a result, I used 3 second contact time to measure the 2D effective affinity of the other TCR mutants.

Similar to findings on TCR-CD3 interaction, these TCR mutants showed no significant change on TCR-pMHC affinity as the effective affinities measured against I-E^k/k5 was comparable for GK, N136A and NP mutants and WT (Figure 13C). The lack of change in TCR-pMHC affinity as a result of TCR mutation did not correlate with trend previously reported using IL-2 as a readout of functional outcome (26). To obtain an adhesion frequency of ~20% to affirm the condition for >90% single bond lifetime measurements (69), I optimized surface density of pMHC and determined 0.1 second contact time to be used for lifetime measurements (Figure 14B). Under force, the WT TCR and the three mutant TCRs all displayed catch-slip behavior with peak lifetime correlating with the functional outcome previously quantified (26). For instance, the NP mutant, which was found previously to have an increase in IL-2 production of ~32% relative to WT, showed an increase of peak lifetime by ~29%. While the N136A mutant, which was found to have a decrease in IL-2 production of 25% relative to WT, showed a decrease of peak lifetime by ~53% (Figure 13D). The agreement between the magnitude of peak lifetime and IL-2 production strongly suggests a close tie between the strength of TCR-pMHC interaction under force and the functional outcome of cells expressing these TCRs. Furthermore, even though these mutations were made on the constant region of TCR to affect its interaction with CD3 subunits, they had a direct impact on TCR-pMHC interaction despite being remote from the pMHC recognition site. Taken together, these findings provide strong evidence of TCR-CD3 extracellular interaction serving as a critical link in the transduction of pMHC recognition signal to the outcome of early TCR signaling, and a disruption to this critical link can affect TCR recognition of pMHC.

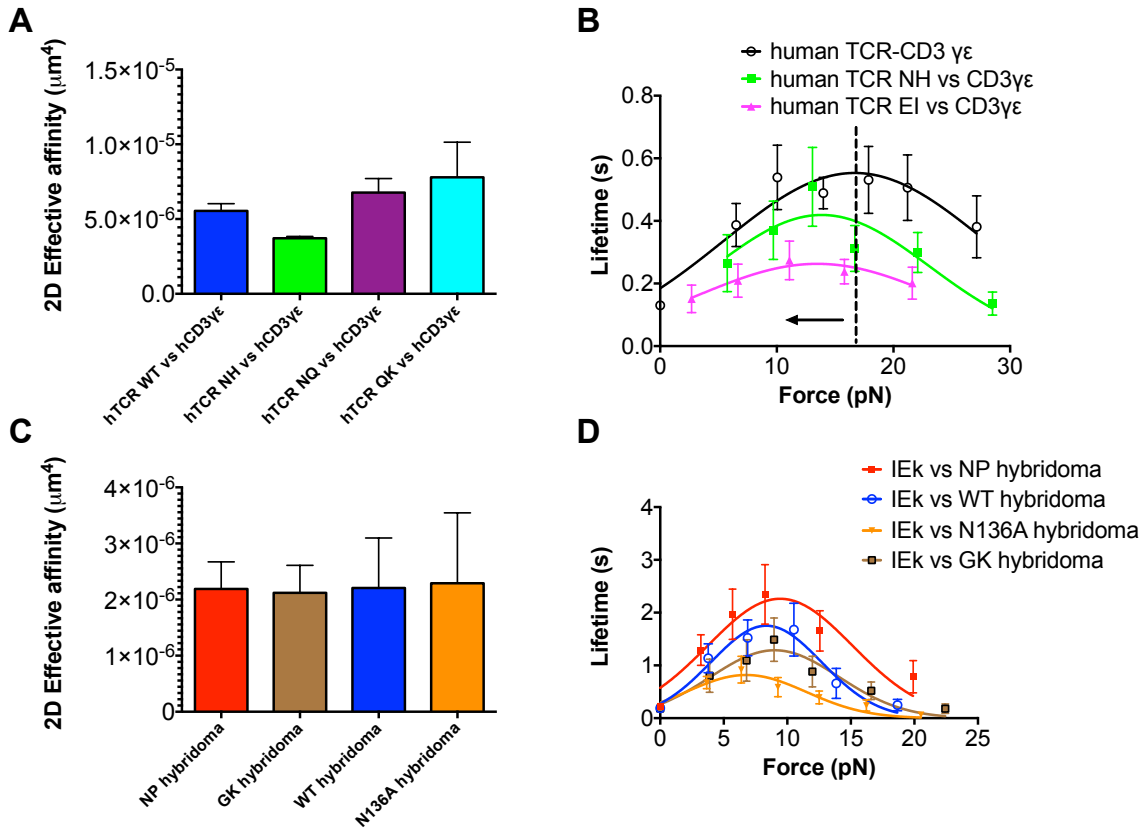

Figure 13 – TCR-CD3 and TCR-pMHC interactions affected by mutations on TCR constant region. (**A**) Mutations on the extracellular domain of TCRβ constant region (NH, NQ, and QK) did not lead to a significant change to the 2D effective affinity. (**B**) Lifetime versus force curves showing TCR NH and TCR EI form catch-slip bonds with human CD3γε, and in comparison to WT TCR, the catch-slip bonds formed between MT TCR and CD3γε have peak lifetime occurring at a lower force, and the magnitude of the catch-slip bond is lower in TCR EI compared with TCR NH. Curves were fitted with Gaussian distribution, and significant differences were found between WT TCR vs CD3γε and TCR NH vs CD3γε interaction curves and between WT TCR vs CD3γε and TCR EI vs CD3γε interaction curves ($p < 0.05$). (**C**) Mutations on the extracellular domain of TCRβ constant region (NP, GK, and N136A) led to no change of 2D affinity between TCR and pMHC loaded with I-E^k/k5. (**D**) Mutations in (**C**) led to a shift in bond lifetime of TCR against I-E^k/k5 under force. Curves were fitted with Gaussian distribution, and significant differences were found between NP and WT, NP and N136A, NP and GK, WT and N136A, and GK and N136A curves ($p < 0.05$). Data are mean ± SEM.

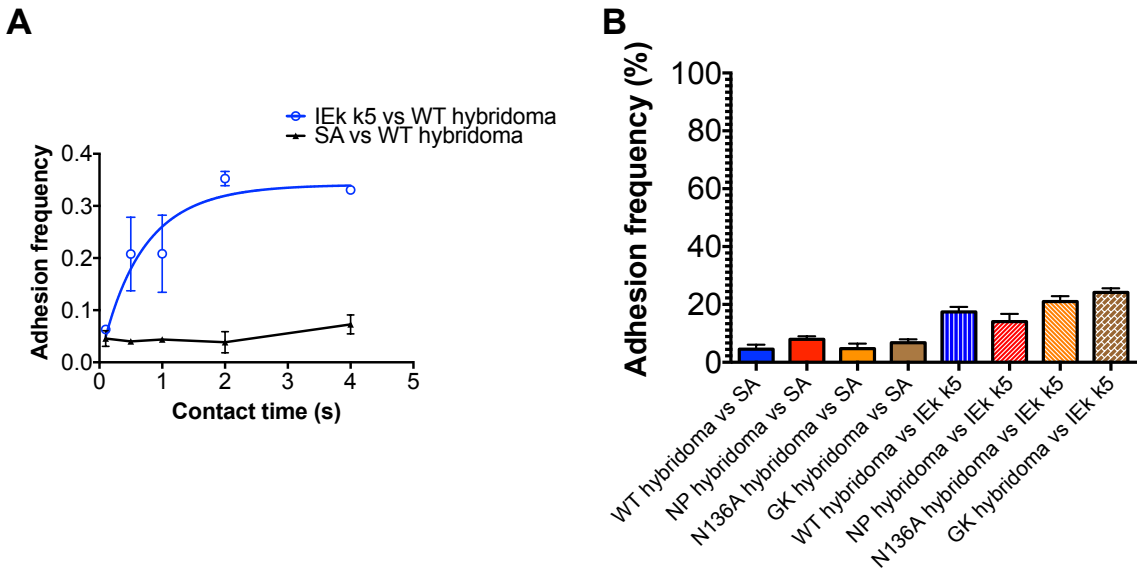

Figure 14 – Adhesion frequency control using beads coated with SA against T cell hybridoma expressing WT and mutant TCRs. (**A**) Adhesion frequency vs time curve of hybridoma expressing WT TCR interaction with pMHC loaded with I-E^k/k5 (blue) and with beads coated with SA (black). (**B**) Adhesion frequency comparison between non-specific control (vs beads coated with SA) and specific interaction against I-E^k/k5 at 0.1 second contact time. Conditions were optimized to attain ~20% adhesion frequency for lifetime measurements using BFP. Data are mean ± SEM.

4.3 Discussion

Findings from this study have demonstrated the presence of specific interaction between TCR and CD3 in the ectodomain through direct measurement in both mouse and human systems. In comparison with mouse TCR binding affinity with agonist pMHCs, which resides in the region of 10^{-4} um^4 in general, the observed TCR-CD3γε interaction and CD3γε homotypic interaction are two orders of magnitude lower and thus considered weak interactions. This could explain why such interactions were not detectable using other methods such as SPR (24). Nevertheless, our sensitive assays have shown that these TCR-CD3 interactions indeed exist.

The presence of ectodomain heterotypic CD3 interactions suggests a potential role of such interactions in facilitating and stabilizing the dimerization of TCR complex, as suggested in a prior EM-based study (21), which proposed a model where CD3 subunits are situated at the center of the dimer with TCRs that are engaged with pMHC on the outside forming an angle with respect to one another. Although these data do not provide definitely proof on the exact orientation of the CD3 subunits around TCR, the potential stabilization effect of dimeric TCR from CD3-CD3 extracellular interactioin is a possible reason for the existence of such an interaction.

Antibody blocking of the FG loop on mouse TCR beta chain significantly reduced the adhesion frequency between TCR and CD3γε, suggesting a major contribution of the FG loop in mediating the extracellular interaction between TCR and CD3. These data therefore support the results of previous studies where potential TCR-CD3 binding sites were proposed based on the crystal structure of αβTCR with H57-597 Fab and results from antibody blocking experiments (19). Furthermore, deletion of the FG loop was found to reduce functional sensitivity of TCR-mediated activation (89), signifying the importance of the FG loop in signal transduction. However, since the antibody did not completely abolish the interaction between TCR and CD3, it is still possible for there to be other extracellular binding sites between TCR and CD3, albeit having minor contribution in comparison with the FG loop. These findings are not exhaustive, other candidates, such as the AB loop of the TCR Cα domain, which has been proposed to regulate TCR dimerization (90), can be worthwhile targets for future studies investigating the effect of point mutations in the AB loop on TCR-CD3 and even TCR-TCR affinities.

Findings presented in this study support the concept that force is critical in T cell triggering and early signaling. Force from actin retrograde flow and myosin-II dependent contraction may be transmitted to TCR bound to anchored pMHC molecules (10), and formation of immunological synapses and kinapses (11, 12, 91). Internal force generated by T cells have been visualized to exert on TCR via engaged pMHC molecules (51, 53). In addition, previous studies (13, 92) have demonstrated the force-dependent kinetics of TCR-pMHC interactions using preTCR and mature αβTCR, and identified the optimal condition at which the lifetime of TCR-pMHC interaction is the longest, leading toward more effective T cell triggering. In naïve OT1 T cells, TCR was found to form a 'catch-slip' bond with agonist pMHCs with an optimal force occurring around 10 pN where the lifetime of TCR-pMHC interaction was found to be the longest before a further increase in force began to decrease bond lifetime (13). This unique 'catch-slip' behavior was only observed in agonistic pMHCs, which could provide a good criterion for separating agonist pMHCs from those with less biological activities, thus aiding TCR discrimination of peptides using the duration of TCR-pMHC interaction under force as a readout. My findings integrate well with the aforementioned study, as they are able to provide insight to the event that occurs immediately following TCR-pMHC interaction, which is the transduction of signal from TCR to the surrounding CD3 subunits in the extracellular domain. The pulling force experienced by the TCR-pMHC interaction is likely relayed to the surrounding CD3 subunits, as evidenced by the prolonged TCR-CD3 lifetime at the same optimal force (10 pN), where the strongest calcium ion flux was triggered in T cells (13). Furthermore, the findings on TCR-CD3 interaction under force show similar trend for both mouse and human systems, although the peak lifetime occurs at a higher force

(~15 pN) for the human proteins, which could be due to the difference in human TCR-pMHC interaction profile under force, a topic that warrants further investigation. A mechanosensing model of TCR was previous proposed (85), which describes the activation of αβTCR by mechanical force through pushing on the CD3ε. Although not directly supported by findings in this study, which primarily involve tensile forces along the interface between TCR and CD3 in the extracellular domain, the importance of a relative positional shift between TCR and CD3 could lead to the same effect of phosphorylation of ITAMs on the cytoplasmic tails of CD3 subunits, as described by the mechanosensing model.

The functional importance on the force-dependent interaction between TCR and CD3 in the ectodomain is highlighted by findings from introducing various point mutations in previously identified TCR-CD3 interaction sites (26). While force-free kinetics between the mutated TCRs and CD3γε molecules failed to correlate with the amount of IL-2 produced upon stimulation when these mutants were expressed in T cells, the magnitude of the catch-slip bond formed by these mutant TCRs with CD3γε showed a more telling change with the lowest IL-2 producer (EI mutant) corresponding to the lowest TCR-CD3γε peak lifetime under force. These findings suggest that despite the similarity in the affinities of TCR-CD3γε interaction of the various TCR mutants under force-free conditions, the ability to prolong interaction under force plays a critical role in dictating downstream responses. Furthermore, these findings showed that even though the locations of these TCR mutations occur in the constant region of the TCR, they can impact the peak lifetime of TCR-pMHC interaction with the magnitude of peak lifetime under force correlating well with IL-2 production upon antigen stimulation as shown previous (26). Despite the fact

that these mutations do not affect TCR recognition of pMHC directly, these findings are unexpected at first glance, but reconcilable, considering the hypothesis that TCR-CD3 extracellular interaction play the role of a relay in the transduction of pMHC recognition signal to intracellular signaling.

Based on previous kinetics studies on the force-dependent nature of TCR-pMHC interaction (13, 93) and my current work, I propose the following model of early TCR signal transduction. Upon engagement with agonist pMHC, the formation of TCR-pMHC catch bond exerts a shearing force along the interface between TCR and CD3 in the ectodomain, resulting in a pulling of CD3 subunits in a direction away from the membrane. The formation of TCR-CD3 catch bond selectively prolongs lifetime of this interaction while TCR is engaged with agonist pMHCs. The prolonged lifetime on CD3 under force permits the transduction of mechanical force across the membrane, which then leads to the swing out of CD3 cytoplasmic tails away from the plasma membrane (27) through possibly force-dependent conformational changes. The exposed CD3 tails allow the phosphorylation of ITAMs by Lck and the subsequent recruitment of Zap70 to phosphorylated ITAMs to initiate other downstream signaling events (94).

Collectively, my findings provide direct evidence to the existence of TCR-CD3 extracellular interaction and the role of such interaction in the transduction of signal from the extracellular arm (TCR-pMHC recognition) to the intracellular arm (early TCR signaling) of the TCR complex. The whole mechanism of how exactly pMHC recognition signal leads to intracellular signaling is by no means solved, as further insights are required on the transmembrane portion and the intracellular portion of the TCR complex in response to force-dependent triggering. Nevertheless, this study is able to fill in an important gap of

knowledge on the extracellular portion of the puzzle and move the field closer toward gaining a complete understanding in a step-wise fashion.

CHAPTER 5. THE CONTRIBUTION OF LCK-DEPENDENT TCR-PMHC-CD8 TRIMOLECULAR INTERACTION IN THYMOCYTE SELECTION

(*Disclaimer: The following work was done in collaboration with Dr. Jinsung Hong (Co-first author). Manuscript in preparation.*)

5.1 Introduction

T cell recognition occurs based on the molecular interaction between T cell receptors (TCRs) displayed on the surface of responding T cells and antigen peptides bound to the major histocompatibility complexes (pMHCs) expressed on antigen presenting cells (APCs). In addition, the invariant CD4 or CD8 coreceptors co-ligate TCR-bound pMHC class II or I molecules, respectively, to provide T-cell specificity (43, 47, 95). This trimolecular interaction is highly elegant in that it does not merely result in an all-or-none response; rather, the responding T cell interprets the information presented by the pMHC, translating the complex input into a broad set of phenotypic outcomes. Since it is vital for T cell recognition, kinetics, structural, and functional studies (41, 42, 47) have been devoted to this molecular interaction. However, our current understanding still is incomplete in how these three molecules interact *in situ* and how such interactions drive T cell function and developmental fate.

Kinetics studies on the TCR-pMHC-CD8 trimolecular interaction so far have been carried out under force-free conditions, using either 3D assays (42, 46) or 2D micropipette adhesion frequency assay (47). Recently, increasing evidence has drawn attention to the

role of mechanical force in TCR–pMHC interaction (11, 86). The role of mechanical force on T-cell activation has been a keen interest since a few surface-bound antigens, unlike soluble form, were able to trigger T-cells (96). Further studies showed TCR-CD3 complex is sensitive to the length of the ligands, such that elongated ligands triggered TCR poorly (17), and rigidity of the surface (97), and calcium signaling was dependent on the mechanical force on TCR or CD3 (16, 17, 98). In addition, traction force from TCR-CD3 complex has been observed using elastomer pillar arrays (99). Our lab recently showed that mechanical force regulates TCR–pMHC dissociation kinetics in a peptide-dependent manner to amplify peripheral T-cell discrimination and trigger calcium signaling (13, 100, 101). Findings from our lab revealed two types of bonds for these interactions: counterintuitive catch bonds where force prolongs their lifetime and ordinary slip bonds where force shortens their lifetime. Furthermore, T-cells showed a ligand dependent generation of pulling force in the presence of CD8 coreceptor, providing the support for the physiological relevance (51).

Based on these previous data that the mechanical force on the TCR and coreceptor is critical for physiological T cell signaling and self vs. non-self discrimination (13, 51, 53, 100, 101), we hypothesize that a major way for force to exert its effect is through the modulation of kinetics of pMHC bonds with TCR and/or CD4/8 for T cell function and development of T-lineage cells. To test this hypothesis, we measured force-dependent lifetimes and molecular stiffness of pMHC bonds with TCR and/or CD8 on thymocytes using a biomembrane force probe (BFP) to determine the quality of bonds (73), in addition to measuring the quantity of bonds at zero force with micropipette adhesion frequency and thermal fluctuation assays (71). We also used DNA-based digital tension probes (50) to

visualize tensile forces generated by thymocytes and exerted on surface-bound pMHCs through TCR and CD8. Lastly, we used CD8.4 hybrid coreceptor and Lck inhibitors to test the contribution of Lck recruitment in these measurements. Our results showed that the quality, not quantity, of the pMHC bonds on thymocytes determines their selection outcomes. We propose a new selection model where thymocytes apply force on TCR and CD8 to elicit Lck-dependent cooperative trimolecular catch bonds (outside-in/inside-out) with negative but not positive selecting ligands, resulting in their differential pMHC engagement times that impact intracellular signaling and apoptosis to generate distinct "live or die" fates.

5.2 Results

5.2.1 The Formation of Lck-Dependent TCR–pMHC–CD8 Trimolecular Interaction Under Force Distinguishes Q4R7 from Q4H7

A previous study from our lab has recently shown that mechanical force amplifies TCR's ability to discriminate agonist and antagonist peptides by forming catch bonds with the former and slip bonds with the latter ligands (13). We therefore used a force-clamp assay (31, 102) to measure the force-dependent bond lifetime (reciprocal of off-rate) (13) (Figure 15A, B) as a metric of bond quality. $CD4^+CD8^+$ double-positive (DP) thymocytes from OTI TCR transgenic mice were used to bind two ligands (Q4H7 and Q4R7) that are neighboring but opposing at the selection threshold (59) to test whether these ligands show different characteristics under force. For both positive selecting ligand Q4H7 and negative selecting ligand Q4R7, the bimolecular interactions of TCR with peptides presented by H2-$K^b\alpha$3A2, a mutation on the α3 domain of the MHC to abolish CD8 binding, showed slip

behavior where bond lifetime decreases monotonically with increasing force (brown circle, Figure 15C, D). The bimolecular interaction of CD8 with VSV:H2-K^b, which is a null peptide for OT1 TCR, was also a slip bond (black triangle, Figure 15C, D). However, when the peptides were presented by H2-K^b to allow for CD8 interaction, distinct trends were observed. Q4H7 still formed slip bonds but Q4R7 formed catch-slip bonds where lifetime first increased, reached a maximum (> 0.4s) around 13pN, then decreased with increasing force (green square, Figure 15C, D).

Since the coreceptor CD8 is known to recruit the Src kinase Lck to the TCR complex during the T cell activation, we tested whether Lck inhibition had any contribution in the formation of catch bond under force. Recent study from Dr. Ed Palmer's group (103) reported the shift of thymocyte selection threshold using a chimeric CD8.4 that has an extracellular portion of CD8 combined with CD4 cytoplasmic tail. The result suggests that higher tendency of recruiting Lck to the proximity of TCR by CD8.4 facilitate higher chance of triggering downstream signaling, thus providing the mechanism for antigen scanning and thymocyte selection. In order to test whether enhancement of Lck connected to the cytoplasmic tail of CD8 may facilitate any augmentation to TCR–pMHC–CD8 complex formation under force, we re-examined OTI CD8.4 system with force-clamp assays. Interestingly, when force was applied to the TCR–pMHC–CD8.4, Q4H7, a positive selecting ligand in the OT1 CD8 system, also behaved like negative selecting ligand Q4R7 and exhibited catch-slip bond (green square, Figure 15E, F). Despite this effect due to increase Lck binding propensity to CD8, the necessity of CD8.4 binding to the H2-K^b was essential to the catch bond, just like in the OTI CD8 system, as bimolecular TCR-pMHC

interaction still showed slip bond (brown circles, Figure 15E, F), indicating that TCR–pMHC–CD8.4 interaction at the extracellular portion is critical for discrimination.

To further test the role of Lck cooperative CD8 binding under force, we preincubated OT1 thymocytes with Lck inhibitor (7-Cyclopentyl-5-(4-phenoxyphenyl)-7H-pyrrolo[2,3-d]pyrimidin-4-ylamine) and ran force-clamp assay in the presence of the inhibitor. Whereas the bond lifetime of positive selecting ligand Q4H7 had minimal effect from the Lck inhibition (green squares, Figure 15G), negative selecting ligand Q4R7 shifted from a catch-slip bond to a slip-bond in the presence of the Lck inhibitor, suggesting the influence of Lck in force-enhanced CD8 cooperativity (green squares, Figure 15H). These findings were corroborated by results from OT1 CD8.4 thymocytes under Lck treatment. Q4H7, which formed a catch-slip bond in the CD8.4 system (black triangles, Figure 15I), exhibited a slip-bond in the presence of the Lck inhibitor, while Q4R7 retained its catch-slip behavior (black trianges, Figure 15J), suggesting that Lck plays a bigger role in aiding the formation of TCR-pMHC-CD8 interaction for weaker ligands, and to a less extend for stronger ligands. Overall, these data support that Lck may facilitate the formation of TCR–pMHC–CD8.4 trimolecular interaction as previously suggested and once those complexes tend to form, force-regulation may determine differential bond lifetimes for selection threshold.

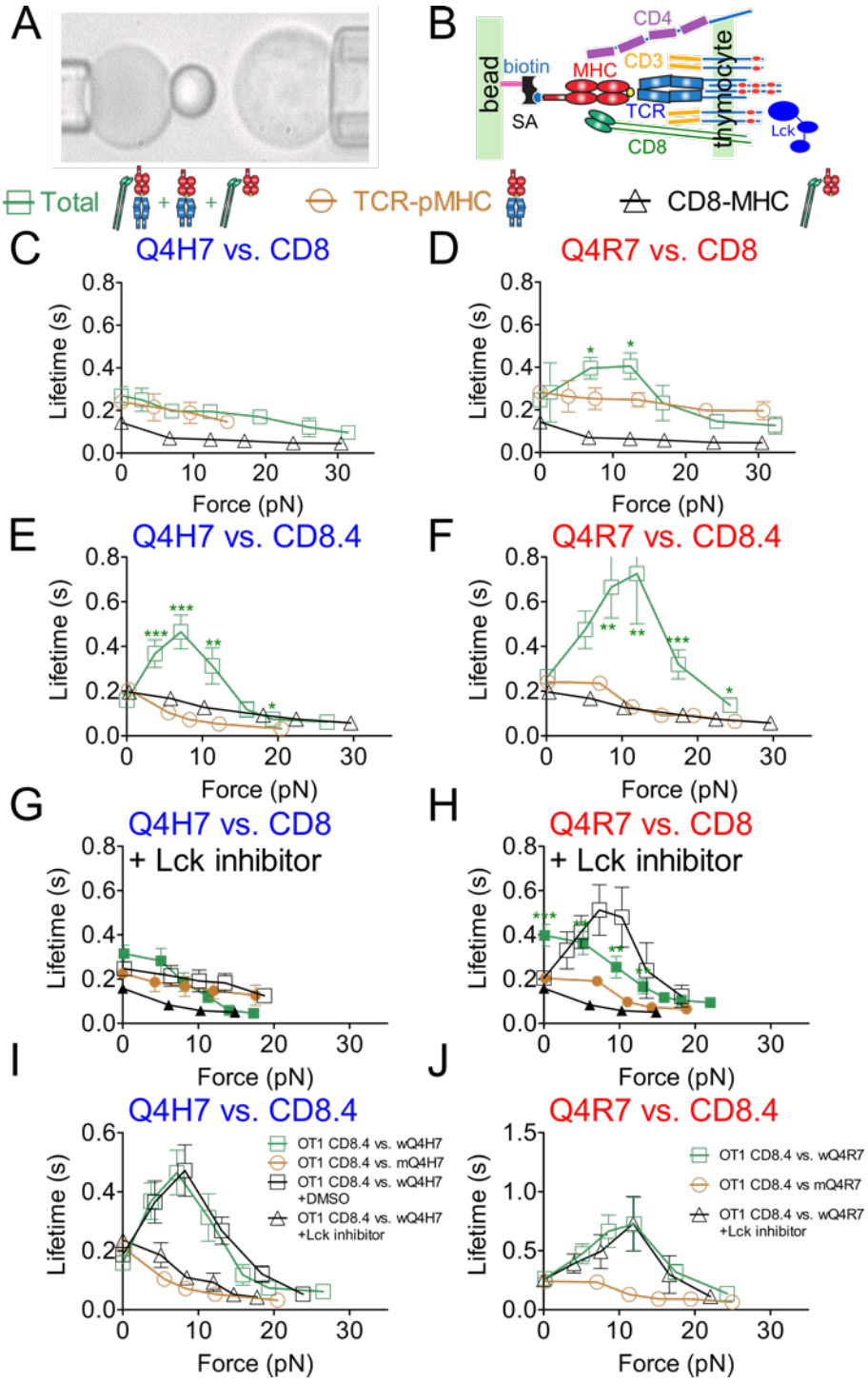

Figure 15 - Distinctive Lck-dependent and force-prolonged lifetimes of OTI TCR and/or CD8 bonds with positive and negative selecting ligands. (A) Micrograph of the BFP setup in force-clamp assays. BFP uses a glass bead to present the pMHC. **(B)** Schematic showing the interacting molecules: pMHC coated on RBC or BFP bead surface via biotin–streptavidin (SA) coupling (left), and the TCR-CD3 complex and CD4 and CD8

coreceptors expressed on the DP thymocyte membrane (right). **(C-J)** Lifetime vs. force plots of TCR bonds with Q4H7 and Q4R7 peptides presented by H2-K^bα3A2 (brown circle), CD8 bond with VSV:H-$2K^b$ (black triangle), and total TCR and/or CD8 bonds presented by H2-K^b (green square) in three different systems, i.e., CD8, CD8,4 and CD8 with Lck inhibitor. Purple square indicate DMSO control in E and F. Filled symbols in G and H indicate data from Lck treatment. Open triangles indicate data from Lck treatment in CD8.4 system, and open square indicates DMSO control in CD8.4 system. Data are presented as mean ± SEM.

5.2.2 The Stiffness of the Bond Under Force Distinguishes Q4R7 from Q4H7

One interesting finding from the force assay data is that linear superpositions of two TCR–pMHC and MHC–CD8 bimolecular slip bonds cannot produce a catch bond regardless of how their relative contributions are adjusted. The observation of catch bonds therefore indicates the presence of cooperative TCR–pMHC–CD8 trimolecular interactions (104), which were allowed by using H2-K^b to measure total interactions. To directly demonstrate trimolecular bonds and to evaluate their fractions, molecular stiffness was analyzed (Figure 16B-D) (73, 104) as another metric of bond quality. It was reasonable to hypothesize that either TCR–pMHC or MHC–CD8 bimolecular complex (Figure 16E) should be less stiff than the TCR–pMHC–CD8 trimolecular complex (Figure 16F). The histograms of molecular stiffness of MHC–CD8 bimolecular bond in either normal OTI (Figure 16G) or OTI CD8.4 system (Figure 16H), as well as TCR–pMHC bimolecular bonds for Q4H7 (Figure 16I) and Q4R7 (Figure 16K), showed a single mode well-fitted by Gaussian distributions of the same mean (0.17 pN/nm). However, bimodal histograms of molecular stiffness were observed for the total bonds of negative selecting ligand Q4R7 (Figure 16L). The bimodal histogram is statistically better fitted by a double Gaussian distribution (p<0.05, F-test) than the single one with the first mean equal to, and the second mean much stiffer (0.51 pN/nm) than the mean of the mono-modal histograms of the

bimolecular bonds. Interestingly, the molecular stiffness histograms of total bonds for the positive selecting ligand Q4H7 (Figure 16J) remain mono-modal and its double Gaussian fits is no better than single Gaussian fits (p>0.1, F-test). Thus, the presence and absence of a stiffer subpopulation for the respective negative and positive selecting ligands correlates with the presence and absence of trimolecular bonds, and is well-suited as a secondary readout of coreceptor contribution in the formation of trimolecular complex. In addition, while the inhibition of Lck on OT1 thymocytes had no effect on the positive selecting ligand Q4H7 histogram (Figure 16Q, R), it eliminated the stiffer population in the total bonds of negative selecting ligand Q4R7 (Figure 16S, T), suggesting that the formation of trimolecular interaction cannot occur in the absence of Lck activity.

Interestingly, the molecular stiffness readout applies very well in the CD8.4 system where the selection threshold has shifted, making Q4H7 a negative selecting ligand. For instance, the histogram of molecular stiffness for Q4H7 bound to H2-K^b using CD8,4 system yielded bimodal distribution (Figure 16N) just like that of Q4R7 (Figure 16P), further providing evidence for the enhancement of TCR–pMHC–CD8.4 binding from the enhancement of Lck recruitment. In comparison, CD8.4 system testing TCR–pMHC bimolecular bonds for Q4H7 (Figure 16M) and Q4R7 (Figure 16O) show only a single mode Gaussian distribution.

Overall, our findings on molecular stiffness demonstrated that bimolecular bonds, are well-characterized by a single mode Gaussian distribution, while the presence of both bimolecular and trimolecular interactions, formed exclusively by negative selecting ligands, results in a bimodal distribution with the second peak occurring at a higher stiffness value. The presence of the second peak from molecular stiffness analysis

combines well with the force vs lifetime results and serves as a good indicator for the presence of trimolecular interactions.

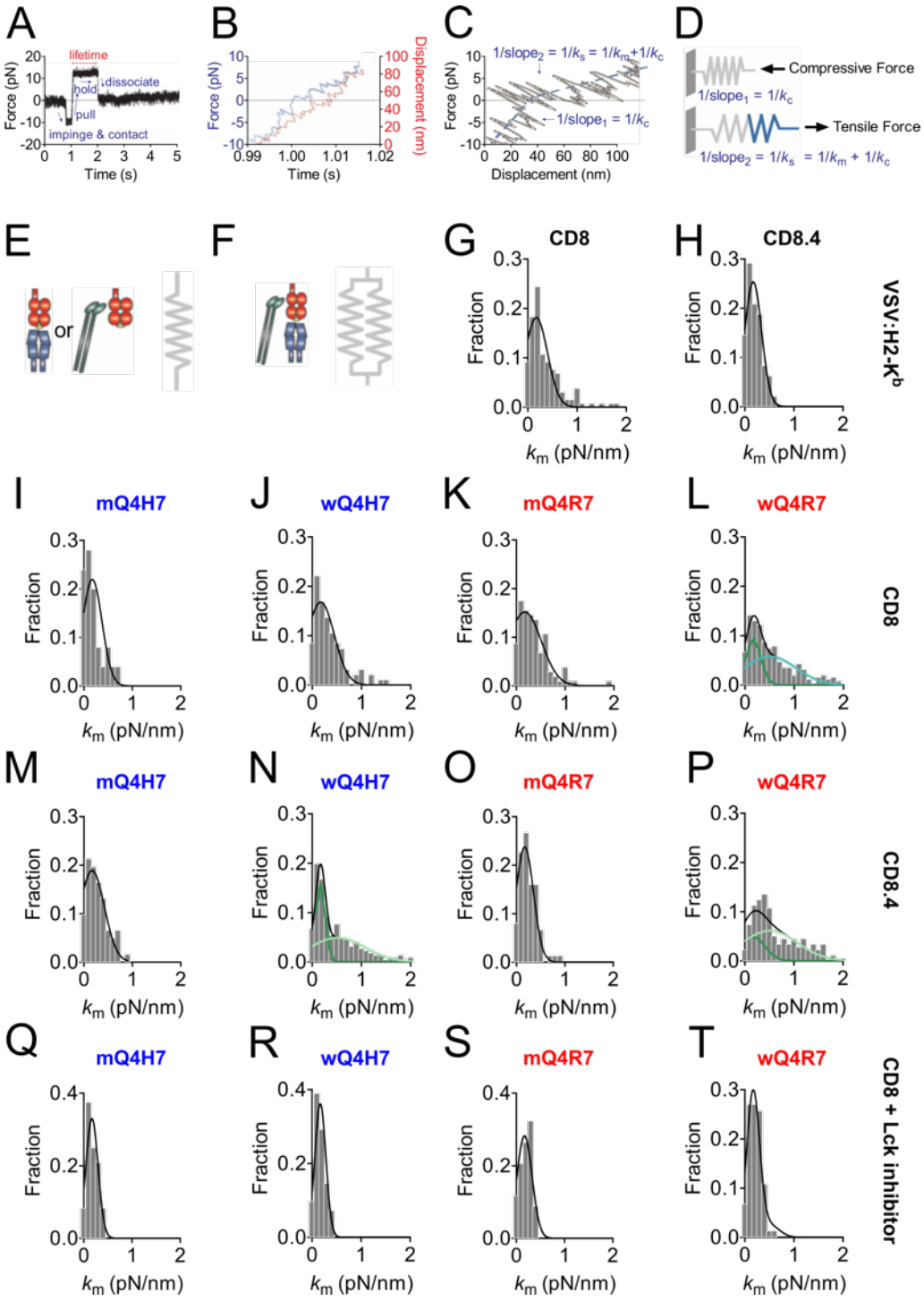

Figure 16 - Molecular stiffness analysis reveals trimolecular bonds with negative but not positive selecting ligands. (A) Force vs. time trace of a BFP force-clamp assay representing a typical test cycle indicating thymocyte impingement from its contact with the BFP bead, retraction of the bead to release compression and pulling of the molecular interaction with a ramp tension, and holding at a pre-determined clamp force for lifetime

measurement until bond dissociation. **(B)** Force (left ordinate, blue) and displacement (right ordinate, red) vs. time traces corresponding to the ramping portion in **A**. **(C)** Force vs. displacement trace obtained by combining the two traces from **B** to eliminate time. **(D)** Illustration of how molecular stiffness is determined from direct measurement. Two line segments (blue dashed lines, **C**) were fit to data to allow for evaluation of the slopes. Their reciprocals equal, respectively, the compliance of the cell in compression, $1/k_c$, and the sum of compliances of the molecule and of the cell in tension, $1/k_m + 1/k_c$. **(E)** Mechanical model (two springs in parallel) for the TCR–pMHC–CD8 trimolecular complex. **(F)** Mechanical model (spring) for the TCR–pMHC and MHC–CD8 bimolecular complex. **(G, H)** Molecular stiffness histograms of CD8 and CD8.4 bonds with VSV:H2-K^b. **(I-T)** Molecular stiffness histograms in CD8, CD8.4 and CD8 with Lck treatment system of OTI TCR bonds with Q4H7 and Q4R7 peptides presented by H2-K^bα3A2 (**I, M, Q** for Q4H7 and **K, O, S** for Q4R7); and total TCR and/or CD8 bonds with peptides presented by H2-K^b (**J, N, R** for Q4H7 and **L, P, T** for Q4R7). Data (bar) were fitted globally by a single (black curve) or double (black curve = green curve + cyan curve) Gaussian with the same soft (0.17pN/nm) and stiff (0.51pN/nm) means for all panels but with different standard deviations and different fractions for the soft and stiff subpopulations. F-test shows the double Gaussian distribution fit the data significantly better than the single Gaussian distribution for Q4R7 ($p<0.002$) but not for Q4H7 ($p>0.1$).

5.2.3 Thymocytes Pull More on Q4R7 via Both TCR and CD8 But Less on Q4H7 via TCR Only to Induce Differential Functionalities

Our data thus far have demonstrated the crucial role of force by applying it externally via a BFP. We next tested the hypothesis that thymocytes exert internally-generated force on the TCR and coreceptor to pull on pMHC on the APC surface, thereby eliciting catch and slip bonds to determine their fates. We tagged pMHC with a DNA-based digital tension probe whose DNA-hairpin unfolds at a designed tension (chosen to be 4.7 or 13.1 pN) to de-quench a Cy5 fluorophore (Figure 17A), thereby reporting an above threshold force applied to the ligand (Figure 17B-D) (50, 51). As reported previously, we observed inefficient thymocytes spreading on the glass surface (105) which led to relatively low frequency of Cy5 positive signaling (<10%). Of those, we managed to find thymocytes that formed multifocal immunological synapse (106) which showed signaling for Q4H7 and Q4R7.

The differences between fluorescence signals for peptides bound to H2-$K^b\alpha$3A2 (Figure 17E) and H2-K^b (Figure 17F) report the number of cooperative TCR–pMHC–CD8 trimolecular bonds pulled by thymocytes with >13.1pN of forces. Thus, upon ligand recognition by the TCR, the CD8 was induced to pull on Q4R7 (red, Figure 17F) but not on Q4H7 (blue, Figure 17F). In addition to comparing different thymocytes at a fixed time point, we also followed the same thymocytes over 10 minutes after initial surface contact (Figure 17G, H). The fluorescence signal decayed over time more slowly on H2-K^b bound to Q4R7 than Q4H7 (Figure 17H), demonstrating that thymocytes exert more sustained forces on negative selecting ligands compared to positive ones. Using H2-$K^b\alpha$3A2 to prevent CD8 binding greatly accelerated the decay of force signal for Q4R7 but not so much for Q4H7, as it was fast even in the H2-K^b condition (Figure 17G). This shows that CD8 binding is required for thymocytes' more sustained pulling on negative selecting ligands. It also reveals that CD8 binding plays a minimum role in thymocytes' pulling on positive selecting ligands. In comparison, with the increase in Lck association to corecptor CD8, the results from OTI CD8.4 system showed the Q4H7 bound to H2-K^b (Figure 17J) but not H2-$K^b\alpha$3A2 (Figure 17I) displayed higher Cy5 intensity comparable to that of Q4R7. The fluorescence signal decay also showed the similar effect where Q4H7 bound to H2-K^b (Figure 17K), but not H2-$K^b\alpha$3A2 (Figure 17L), had a more sustained signal with slower decay similar to that from Q4R7. In addition, whereas the inhibition of Lck had no effect on the Cy5 intensity of positive selecting ligand Q4H7 (Figure 17M, O), it eliminated the higher Cy5 intensity in the negative selecting ligand Q4R7 (Figure 17N, P). Therefore, Lck was found to be responsible for inducing CD8 synergizes with the TCR to enable thymocytes to generate sustained pulling force on negative but not positive selecting

ligands, as when Lck signaling or CD8 binding was prevented, the significant differences between force signals for Q4R7 and Q4H7 vanished. Thus, the differences between fluorescence signals for peptides bound to H2-K^b and H2-$K^b\alpha$3A2 (Figure 17F minus E, Figure 17J minus I, and Figure 17N minus M values for matched ligands) report the number of cooperative TCR–pMHC–CD8 trimolecular bonds pulled by thymocytes with >13.1pN of forces. Taken together with the force vs. lifetime data and molecular stiffness analysis, DNA force probe results provide a third orthogonal readout highlighting the contribution of CD8 in TCR-pMHC-CD8 trimolecular interaction in a Lck-dependent manner through a direct visualization of pull force exerted by TCR and/or CD8 on pMHC molecules.

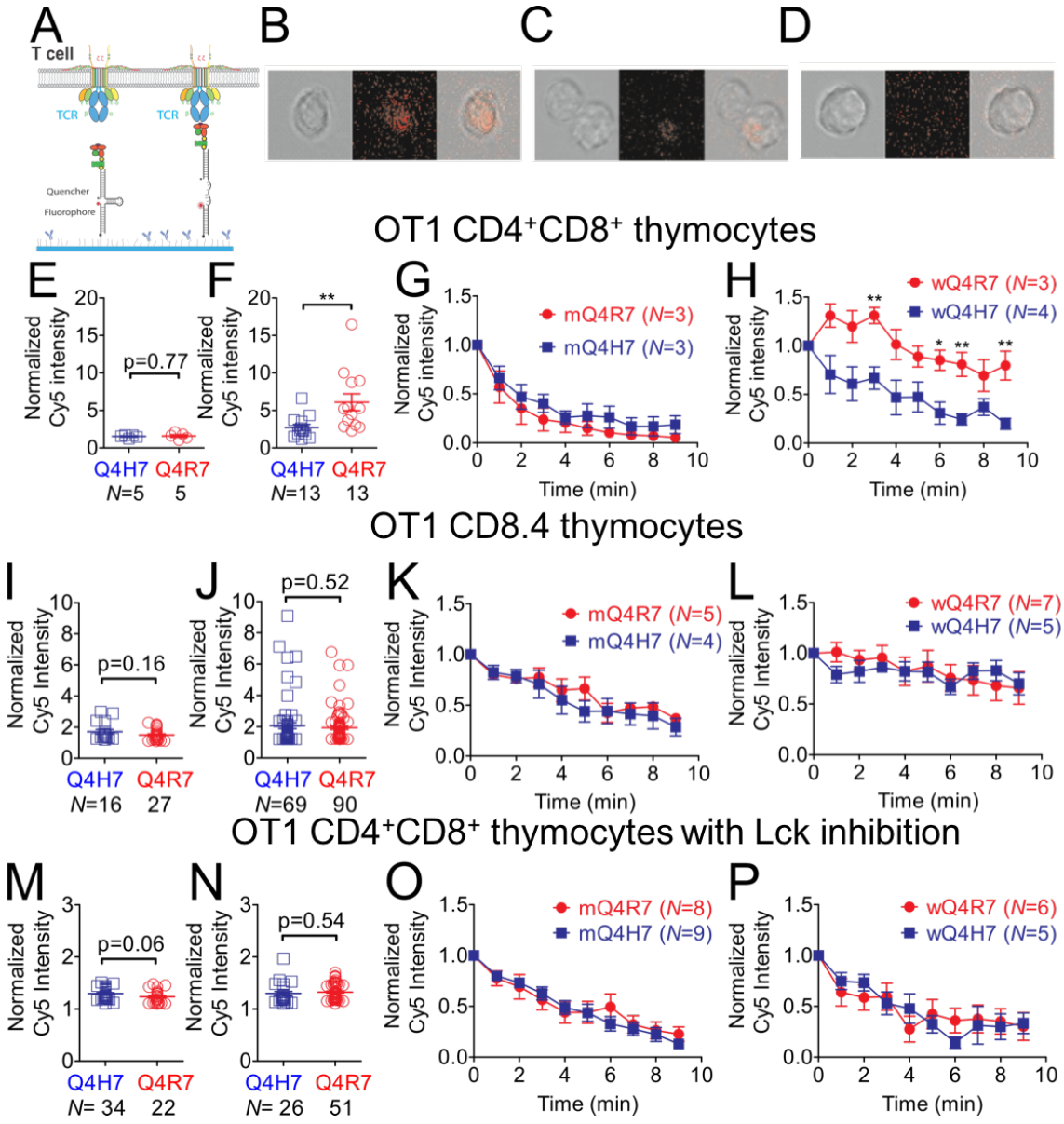

Figure 17 - Thymocytes pull on TCR and CD8 engaged with Q4R7 but not with Q4H7. **(A)** Schematic image of pMHC-connected single hairpin DNA force probe engaging with TCR complex. (**B-D**) Representative thymocyte images on Q4R7 (**B**), Q4H7 (**C**), and VSV (**D**) tagged with a 13.1pN DNA force probe viewed in the bright-field (left column), fluorescence (middle column), and merged (right column) channels. (**E, F** for CD8; **I**, **J** for CD8.4; **M, N** for CD8 with Lck treatment) Quantitative comparison of normalized fluorescence intensity for indicated peptides bound to H2-K^{b}α3A2 (**E, I, M**) or H2-K^b (**F, J, N**). Normalized fluorescence intensity was calculated by dividing the mean fluorescence intensity from a Cy5 positive (above the VSV control) cell by the background calculated from single cell-sized ROI. Each positive signaling cell is presented by a circle with mean ± s.e.m. of all positive cells. (**G, H** for CD8; K, L for CD8.4; **O, P** for CD8 with Lck treatment) Normalized fluorescence intensity decay in selective area of Cy5 signal of

thymocytes on indicated peptides bound to H2-K^{b}α3A2 (**G, K, O**) or H2-K^b (**H, L, P**). For quantitative comparison, the normalized fluorescence intensities post background subtraction were normalized again by the value at the initial time (t = 0 minute). Data are presented with mean ± SEM. normalized fluorescence intensity. Student's t-test was used for statistical analysis at each time point.

5.2.4 Lck-dependent TCR-pMHC-CD8 interaction under force distinguishes thymocyte selection

The comparison between Q4H7 and Q4R7 in bond lifetime measurement, stiffness analysis, and DNA force probe experiments suggested that TCR-pMHC-CD8 interaction may have a distinct threshold for thymocyte selection. Thus, we tested additional ligands that span across the selection boarder. Consistent with previous observation using Q4H7 and Q4R7, slip bonds were observed for positive selecting ligands (Figure 18D-F) including endogenous ligands (60, 61) (Figure 18F). However, in the case of negative selecting ligands, catch bond was observed (Figure 18A-C). Moreover, we verified our observation in another TCR system (2C), confirming that negative selecting ligands form catch-slip bonds with longer bond lifetime whereas the positive selecting ligands formed slip bonds (Figure 19A).

Furthermore, the stiffness analysis showed the presence of bimodal distribution for negative selecting ligands whereas only single distribution for positive selecting ligands (Figure 18E). When calculating the bond fraction, trimolecular bond fraction ϕ_t increases with the ligand biological activity at the expense of the bimolecular bond fraction ϕ_b (to satisfy $\phi_b + \phi_t = 1$) (Figure 18I), suggesting that the cooperative binding is peptide-dependent and hence TCR-induced. These observations have been confirmed by Dr. Jinsung Hong (former member of our lab) using the 2C TCR (Figure 19E). Regardless of

the peptides, the data of TCR–pMHC bimolecular bonds fitted well by a single Gaussian. For the negative selecting ligands, the data of total TCR and CD8 bonds fitted by a double Gaussian significantly (p<0.01, F-test) better than single Gaussian, whereas for the positive selecting ligands, the total bond data were fitted equally well by a single or double Gaussian distribution, i.e., there are no statistical differences (p>0.1, F-test) in the χ_v^2 values that measure the goodness-of-fit.

In addition, to identify the dissociation characteristics of the stiff and soft fractions of bonds, we analyzed the lifetime distributions of total bonds with a two-state model (107). The model assumes that the total bonds consist of two subpopulations, one short-lived (fraction ω_1) and the other long-lived (fraction $\omega_2 = 1 - \omega_1$), with respective fast and slow off-rate k_{off1} and k_{off2}. The lifetime distributions measured under 10-15pN of forces were fitted by the two-state model (Figure 18J) and the state fractions ω_1 and ω_2 are shown in Figure 18K. The resemblance between Figure 18I and Figure 18K provides further support for the assertion that stiffer bonds are longer-lived.

Lastly, DNA-based digital tension sensor experiments showed that the thymocytes pull on ligands in a selection dependent manner. Except for the noncognate VSV, both Catnb and OVA peptides demonstrated Cy5 signaling indicating the TCR-specificity of these force signals (Figure 18L-N). Importantly, the ability for a ligand to form catch bonds correlates with its ability to induce sustained pulling by thymocytes. This correlation was observed not only on the trimolecular catch bonds of the negative selecting ligands formed with both the TCR and CD8 (Figure 18O) but also on the bimolecular catch bond of the antigenic ligand OVA formed with the TCR only (Figure 18A), as sustained forces were also observed on OVA:H2-$K^b\alpha$3A2 (Figure 18Q). Only background fluorescence was

observed when thymocytes were placed on VSV:H2-K^b surfaces (Figure 18L, O), indicating that without TCR recognition, thymocytes were unable to exert appreciable force on CD8 alone. In addition, using lower force threshold DNA probe (4.7 pN) further supported our observation (Figure 19B-D). Furthermore, the de-quenching Cy5 signal was diminished over time when the actin filaments were disrupted by Latrunculin A or when myosin contraction was prevented using the ROCK inhibitor Y-27632 (Figure 19F, G), indicating that pMHCs were pulled by actomyosin-based forces generated by the thymocytes. This observation is consistent with prior studies highlighting the role of actin polymerization and myosin II-dependent contraction in transmitting force to TCR bound to pMHC (10-12, 108). Thus, upon ligand recognition by the TCR, thymocytes exert actin/myosin-dependent force to induce the CD8 to engage in the formation of trimolecular interaction and pull on negative selecting ligands preferably but not on positive selecting ligands.

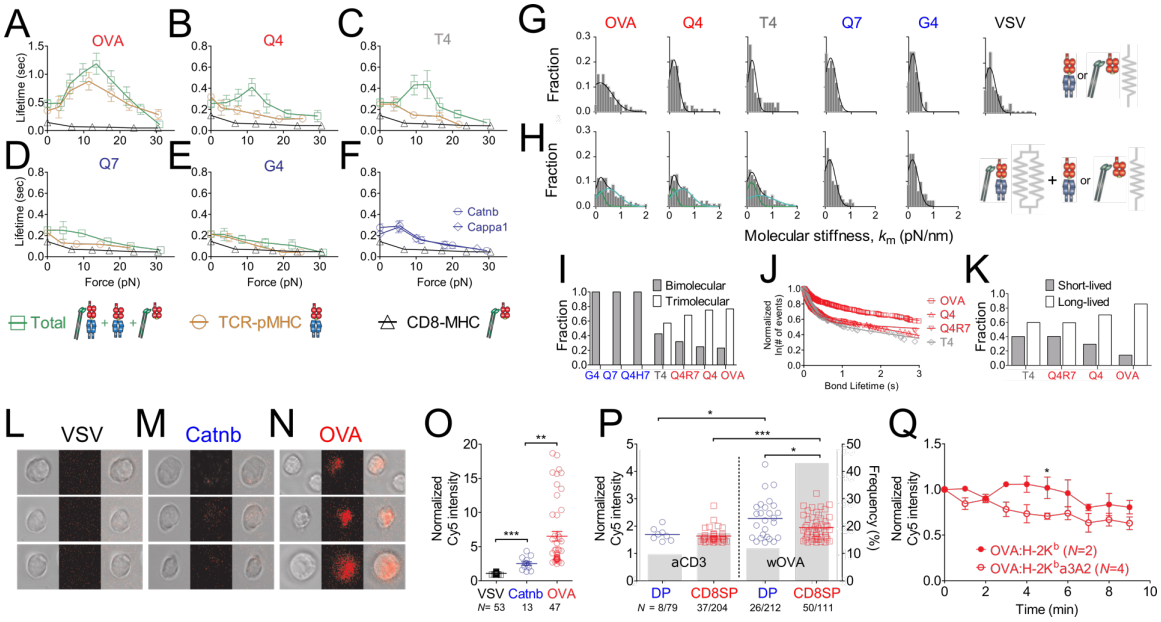

Figure 18 – Distinctive Force-dependent lifetime of OT1 TCR and/or CD8 Bonds with Positive and Negative Selecting Ligands. (A-E) Lifetime vs. force plots of TCR bonds with OVA, Q4, T4, Q7, and G4 peptides presented by H2-K^{b}α3A2 (brown circle), CD8 bond with VSV:H-2K^b (black triangle), and total TCR and/or CD8 bonds presented by H2-K^b (green square). (**F**) Lifetime vs. force plots of TCR bonds with endogenous peptides Catnb and Capp1 (blue) and CD8 bond with VSV:H-2K^b (black triangle**). (G,H)** Molecular stiffness histograms of OTI TCR bonds with OVA, Q4, T4, Q7, G4, and VSV peptides presented by H2-K^{b}α3A2 (**H**); and total TCR and/or CD8 bonds with peptides presented by H2-K^b (**G**). Data (bar) were fitted globally by a single or double Gaussian with the same soft (0.17pN/nm) and stiff (0.51pN/nm) means for all panels but with different standard deviations and different fractions for the soft and stiff subpopulations. (**I**) Fraction of bimolecular and trimolecular interaction formed by OT1 thymocyte with positive selecting (blue) and negative selecting (red) ligands obtained from Gaussian fitting of spring constant analysis. (**J**) Normalized lifetime distribution of total 2D TCR and/or CD8 bonds with H2-K^b bound to the indicated peptides measured at 10-15 pN by force-clamp assay. (**K**) Fraction of short-lived (gray bar) and long-lived (white bar) bonds from fitting with two-state model (107). (**L-N**) Representative images of VSV (**L**), Catnb (**M**), and OVA (**N**) tagged with a 13.1pN DNA force probe viewed in the bright-field (left column), fluorescence (middle column), and merged (right column) channels. (**O**) Quantitative comparison of normalized fluorescence intensity for VSV, Catnb and OVA. (P) Quantitative comparison of normalized fluorescence intensity (points, left ordinate) and fraction of positive cells (bars, right ordinate) for anti-CD3 and OVA in DP thymocytes and SP splenocytes. (Q) Normalized fluorescence intensity decay in selective area of Cy5 signal of thymocytes on OVA peptides bound to H2-K^{b}α3A2 (open circle) or H2-K^b (solid circle).

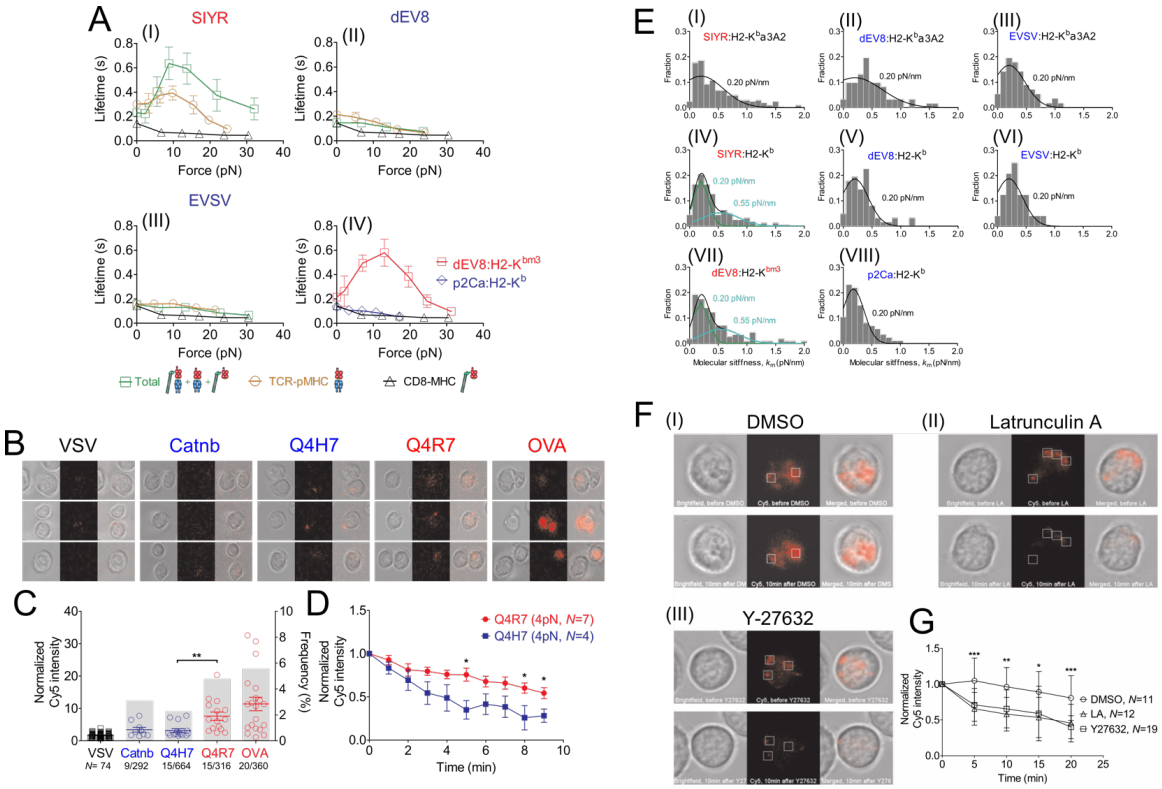

Figure 19 - Distinctive force-dependent lifetime of 2C TCR and/or CD8 bonds with positive and negative selecting ligands and thymocyte pulling reported by 4.7 pN DNA force probe. (A) Lifetime vs. force plots of TCR bonds with SIYR, dEV8, and EVSV peptides presented by H2-K^{b}α3A2 (brown circle), CD8 bond with VSV:H-2K^b (black triangle), and total TCR and/or CD8 bonds presented by H2-K^b (green square). Lifetime vs. force plots of total TCR and/or CD8 bonds with dEV8:H-2K^{bm3} (red square) and p2Ca:H-2K (blue diamond). (Data obtained by Dr. Jinsung Hong) (**B**) Representative thymocyte images on indicated ligands tagged with a 4.7pN DNA force probe viewed in the bright-field (left column), fluorescence (middle column), and merged (right column) channels. (**C**) Quantitative comparison of normalized fluorescence intensity (points, left ordinate) and fraction of positive cells (bars, right ordinate) for indicated peptides bound to H2-K^b. Normalized fluorescence intensity was calculated by dividing the mean fluorescence intensity from a Cy5 positive cell by the background. Data are presented as mean ± SEM of all positive cells (each cell is represented by a circle with $N \geqslant 9$ from at least 292 total cells). Asterisks (**) denotes $p<0.01$ from Student's t-test. (**D**) Normalized fluorescence intensity decay in selective area of Cy5 signal of thymocytes on indicated peptides bound to H2-K^b. For quantitative comparison, the normalized Cy5 intensities were normalized again by the value at the initial time (0min). Data are presented with mean ± SEM. of normalized fluorescence intensity. Asterisks (*) denotes $p<0.05$ from Student's t-test. (**E**) Molecular stiffness histograms of 2C TCR bonds with SIYR, dEV8, and EVSV bound to H-2K^{b}α3A2 (I-III), total TCR and/or CD8 bonds with these peptides (IV-VI) and p2Ca bound to H-2K^b (VII) or dEV8 bound to H-2K^{bm3} (VIII). Data (bar) were fitted globally by a single or double Gaussian per panel with the same soft (0.20pN/nm) and stiff

(0.55pN/nm) mean(s) for all panels but different panels could have different standard deviations and different fractions for the soft and stiff subpopulations. (Data analyzed by Dr. Jinsung Hong) (**F**) Representative thymocyte images on OVA:H2-K^b tagged with a 13.1pN DNA force probe treated with DMSO control (I), an actin polymerization inhibitor latruculin A (II), and a ROCK inhibitor Y-27632 (III). Thymocytes before (top row) and 10min after (bottom row) the drug treatment were viewed in the bright-field (left column), fluorescence (middle column), and merged (right column) channels. (**G**) Normalized fluorescence intensity decay in selective area of the Cy5 signal (normalized again to the value at the initial time point) over 20min. Data are presented with mean ± SEM of normalized fluorescence intensity ($N \geq 11$ ROI from more than 6 thymoyctes pooled from at least two independent experiments). Statistical analysis (one-way ANOVA) is performed as denoted (* = $p<0.05$; ** = $p<0.01$; *** = $p<0.001$).

5.2.5 Disruption of Lck association with CD8 abolishes synergistic TCR-pMHC-CD8 trimolecular interaction

Since we have found earlier that increasing Lck association with coreceptor CD8 favors the formation of TCR-pMHC-CD8 interaction and inhibition of Lck activity abolished trimolecular interaction for ligands near the selection threshold, we went further to test the robustness of our findings by abolishing the interaction between Lck and CD8. Using hybridoma cells expressing OT1 TCR and CD8 with a mutation on the intracellular CxCP motif that abolishes the interaction between CD8 and Lck (44), we measured force-dependent lifetime of these cells and compared that with its non-mutated counterpart. As expected, we found that CxCP mutation abolished catch-slip behaviour of Q4R7, a negative selecting ligand, in comparison to WT cells without the mutation. With the mutation, the magnitude of bond lifetime under force of Q4R7 presented on H2-K^b MHC was comparable to that measured between WT cells and Q4R7 presented on H2-K^b α3A2 condition, where CD8 interaction with MHC was not possible (Figure 20A). This result suggests that despite having an intact extracellular portion of CD8 for binding to MHC, trimolecular interaction was not formed in the absence of Lck association with CD8. When

OVA peptide was presented by H2-K^b MHC, the force vs. lifetime curves exhibited similar catch-slip bond for both WT OT1 hybridoma and the CxCP mutatant (Figure 20). This result is consistent with the force-dependent lifetime measurement carried out using OT1 thymocyte against OVA pMHC. such that preventing CD8-MHC interaction using H2-K^b α3A2 does not result in the abolishment of catch-slip behaviour, indicating that for strong peptides, such as OVA, trimolecular interaction involving CD8 plays a minimal role in regulating force-dependent lifetime. The high potency of the OVA peptide is probably strong enough to surpass the selection threshold without the help of CD8 coreceptor, which plays a more critical role in discriminating ligands near the threshold.

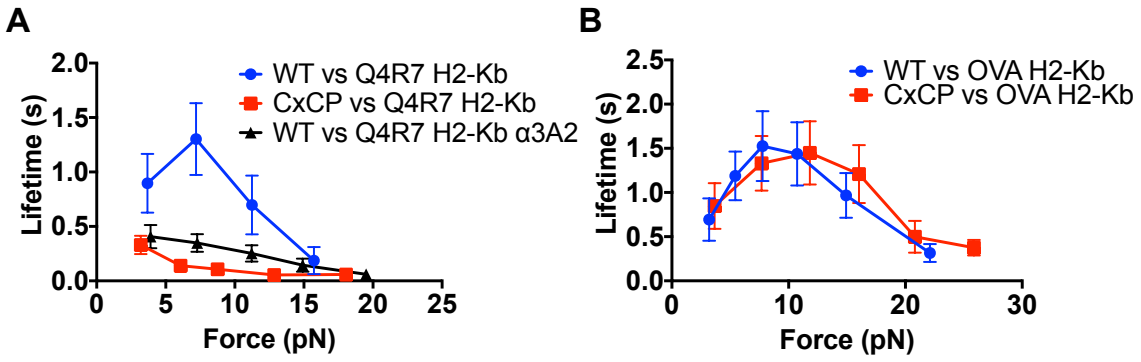

Figure 20 – Abolishing Lck-CD8 interaction with CxCP mutation prevents trimolecular interaction and affects catch-slip behavior of threshold ligand. (A) Lifetime vs. force plot of OT1 hybridoma WT (blue) and CxCP mutant (red) interacting with Q4R7 presented by H2-K^b MHC, and WT interacting with Q4R7 presented by H2-K^b α3A2 (black). **(B)** Lifetime vs. force plot of OT1 hybridoma WT (blue) and CxCP mutant (red) interacting with OVA presented by H2-K^b MHC. Data are presented as mean ± SEM.

5.2.6 Reduction in the number of Lck substrates lowers synergistic TCR-pMHC-CD8 trimolecular interaction

In T cell signaling, Lck phosphorylates ITAMs found on the cytoplasmic tails of CD3. Since our findings so far strongly suggested a dependency of TCR-pMHC-CD8

trimolecular interaction on the activity of Lck, we went a step further to test the impact of reducing the number of Lck substrates per TCR. We utilized thymocytes from OT1 mice with 6F mutation where six out of ten ITAMs on the TCR complex were mutated to abolish their signaling capacity (109, 110). As a result, we observed a leftward shift of bond lifetime against Q4 and Q4R7, two negative selecting ligands, in comparison to regular OT1 thymocytes (Figure 21A,B). Catch bond was still observed for these two ligands, despite the shift in force vs lifetime profile, indicating that there was a partial suppression on the formation of the synergistic TCR-pMHC-CD8 trimolecular interaction due to the decrease in the number of signaling ITAMs per TCR complex.

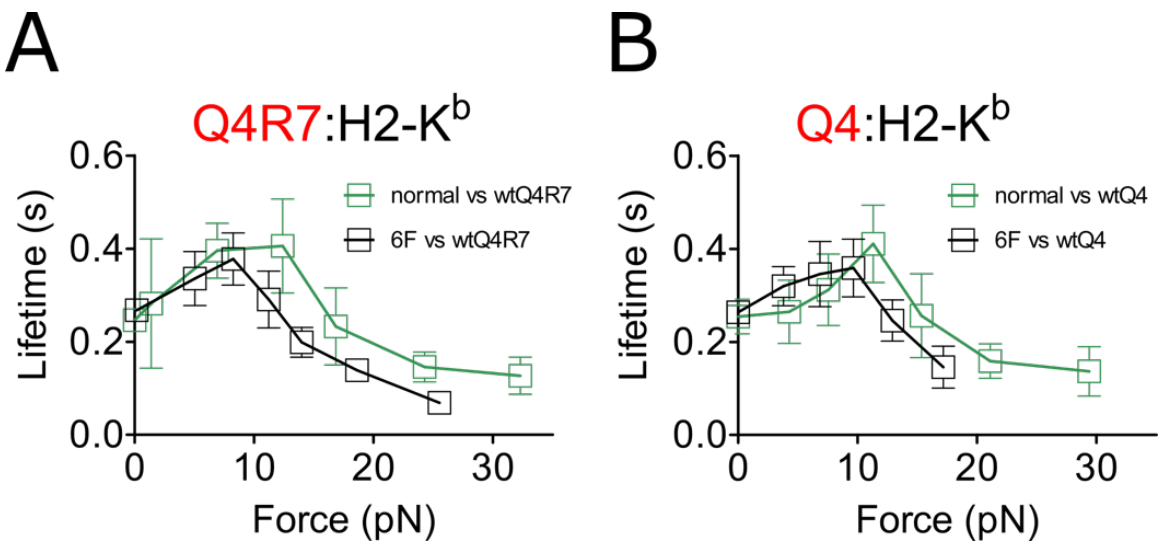

Figure 21 - 6F mutation on CD3 ITAMs reduces the formation of trimolecular interaction. (A, B) Lifetime vs. force plots of OT1 6F TCR and/or CD8 bonds with Q4R7 and Q4 peptides presented by H2-K^b (black square). Data are presented as mean ± SEM.

5.3 Discussion

Our bond lifetime measurements have demonstrated that thymocyte forms catch-slip bond with negative selecting ligands and slip-bond with positive selecting ligands, and

the formation of catch bond is due to the contribution of coreceptor CD8 in forming trimolecular interaction with TCR and pMHC under force, as evidenced by our molecular stiffness analysis. In addition, we visualized force exerted by thymocyte through TCR and/or CD8 on pMHC using DNA force probes, further highlighting the relevance of force in thymocyte selection. We then investigated factors affecting the formation of TCR-pMHC-CD8 trimolecular interaction and found that it requires Lck association to co-receptor CD8, Lck activity, and the availability of Lck substractes, ITAMs on CD3s, for ligands near the selection threshold, but not potent ligands, such as OVA in the OT1 system.

The role of force in TCR-pMHC interaction has drawn increasing attention in recent years, mostly from evidence obtained from studies of mature T cells (13, 51, 99), in the context of thymocyte, however, the contribution of force has not been thoroughly investigated. Thymocyte selection, a critical step in thymocyte development that is primarily mediated by TCR-pMHC interaction, is likely a target subjected to the influence of mechanical forces. As expected, we found that thymocytes form catch bonds with negative selecting ligands exclusively but not the positive selecting one, which could be a novel criterion for ligand discrimination that is only possible under force. CD8 contribution in the formation of TCR-pMHC-CD8 trimolecular interaction was found to be responsible behind the catch bond, as positive selecting ligands displayed very similar force-dependent lifetime profile regardless of whether CD8-MHC interaction is prevented by mutation on MHC. In contrast, negative selecting ligands, with the exception of OVA, did not form catch bond in the absence of CD8-MHC binding. To demonstrate that thymocytes are capable of exerting forces, we utilized DNA force probes to fluorescently report pulling

forces exerted by thymocytes through TCR and CD8 on pMHC, and we found that thymocytes are capable of generating such pulling force, and these forces are dependent on actin and myosin, consistent with prior findings on mature T cells (12, 108).

T cell triggering is commonly thought of as primarily outside-in, with input from pMHC sensed by TCR and CD8 dictating T cell responses. Interestingly, our findings revealed an inside-out component of T cell triggering. Lck association with coreceptor CD8 and Lck catalytic activities are both influencing factors impacting the formation of CD8-MHC interaction as part of the trimolecular complex. Despite having no change to the extracellular portion of TCR and CD8, CD8.4 thymocytes recognize peptides different from CD8 thymocytes, and the difference is manifested by the shift of selection threshold (111) and formation of catch-slip bond by Q4H7, a previously positive selecting ligand. Modifications on the intracellular portion of CD8 is thought to be downstream of TCR-pMHC recognition in the outside-in signaling pathway, and is not expected to alter peptide recognition if TCR triggering is exclusively outside-in. Therefore, the change in peptide recognition by CD8.4 thymocytes strongly suggests that rather than a unidirectional outside-in pathway, TCR triggering has an inside-out component forming a loop. Based on existing data from our experiments and from the field, we propose the following model of TCR outside-in/inside-out loop. The outside-in component consists of two dimeric interactions, one between TCR and pMHC, and the other between CD8 and MHC. The inside-out loop consists of CD8 in association with Lck, which in turn associates with CD3 tails of the TCR complex. Upon receiving the readout from the outside-in component, the cytoplasmic tails of CD3 dissociates from the plasma membrane (27) and becomes available for binding to Lck, resulting in phosphorylation of ITAMs by Lck. As Lck

molecules are recruited to the TCR complex through association with CD8 (112), the interaction between between Lck and CD3 helps to keep CD8 in the proximity of TCR and increases the chance of CD8-MHC interaction and promotes rebinding of CD8 to existing TCR-pMHC interaction, thus favoring the formation of trimolecular interaction (Figure 22). Essentially, the inside-out component provides an additional level of check through favoring the formation of trimolecular interaction with certain peptides, resulting in prolonged lifetime of interaction of TCR with these peptides surpassing a certain threshold, leading to differential cellular responses from the T cell.

It remains unclear exactly how does TCRs on thymocyte differentiate pMHCs prior to the onset of CD8-MHC binding, since force-dependent lifetime shows comparable profile and magnitude of TCR-pMHC interaction for ligands across the selection threshold, and we speculate that small differences in the outside-in readout get amplified by the inside-out component of the TCR signaling loop, resulting in a larger difference for T cell decision making. It is worth noting that OVA is able to form catch-slip bond without CD8 participation, and we reason that this exception is due to the high potency of OVA compared to the other peptides tested such that TCR recognition OVA-loaded MHC is able to make signaling decisions without receiving help from CD8 to amplify the outcome from the outside-in portion of the signaling loop. Further effort to investigate this initial difference in TCR-pMHC recognition on thymocyte is warranted to fully understand the events revolving around TCR triggering.

In summary, we have demonstrated the contribution of force in the formation of TCR-pMHC-CD8 trimolecular interaction, resulting in prolonging of the lifetime of interaction with negative selecting peptides. This novel force-dependent readout is capable

of differentiating negative selecting peptides from the positive selecting one, thus acting as a unique criterion for antigen discrimination in the context of thymocyte selection. Furthermore, by investigating the various factors affecting the formation of this trimolecular interaction, we propose a new model of TCR triggering with the addition of an inside-out signaling component creating a signaling loop with the well-known outside-in portion mediated by TCR recognition of pMHC.

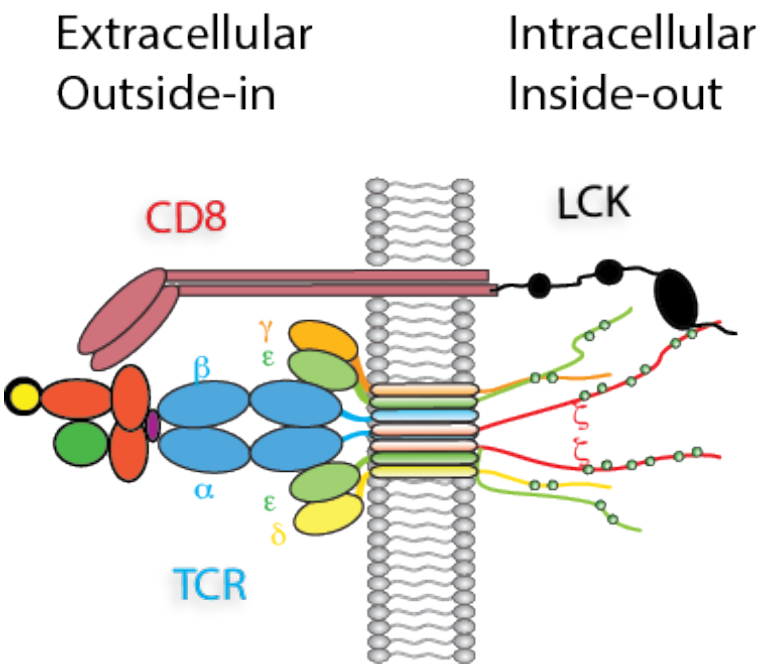

Figure 22 - TCR outside-in/inside-out signaling loop consists of the extracellular outside-in portion involving two dimeric interactions (TCR-pMHC and MHC-CD8), and the inside-out portion containing Lck bridging together CD3 and CD8.

CHAPTER 6. CONCLUSIONS AND FUTURE DIRECTIONS

6.1 Conclusion

I presented in this thesis a two-part study revolving around the role of force in TCR triggering. In the first part, I focused on characterizing TCR-CD3 extracellular interaction and probing the significance of this force-dependent interaction in TCR triggering. In the second part, I investigated the formation of TCR-pMHC-CD8 trimolecular interaction under force in the context of thymocyte selection to relate our findings from the kinetics aspect to functional outcomes affecting cell fate.

In the study of TCR-CD3 interaction, I presented the first 2D kinetics measurement of TCR-CD3 and CD3-CD3 extracelluar interactions. I found that these interactions exhibit catch-slip behavior, with the optimal lifetime of TCR-CD3 interaction occurring at the same force range that gives rise to the longest TCR lifetime with agonist pMHC, suggesting that TCR-CD3 play a potential role of relaying force signal from pMHC recognition end to the intracellular signaling end. Furthermore, I identified that mutations that affect the extracellular TCR-CD3 interaction also impact TCR antigen recognition, thus highlighting the importance of TCR-CD3 extracellular interaction as a critical player in TCR triggering.

In the study of the role of force in the formation of TCR-pMHC-CD8 trimolecular interaction, we identified a novel criterion for thymocytes to discriminate negative selecting ligands from positive selecting ones. Thymocytes were found to form catch-slip bond with negative selecting ligands but not positive selecting ones, and this catch-slip behavior is the result of CD8 contribution to TCR-pMHC interactions. We further

investigated and identified Lck association with Lck and Lck catalytic activities as two important factor determining the formation of CD8-MHC interaction, thus allowing us to formulate a new model of TCR triggering involving not only a unidirectional outside-in portion but also an inside-out component mediated by Lck association with both CD8 and CD3. The inside-out portion selectively favors the participation of CD8 in TCR-pMHC interactions for certain peptides by reacting to the outcome from the outside-in from initial TCR-pMHC interaction.

6.2 Future directions

Findings presented in this thesis contribute to the field in 1) providing direct evidence to identify specific interaction between the extracelluar domains of TCR and CD3, an area that lacked direct measurements previously, and 2) relate TCR-pMHC-CD8 trimolecular interaction to the functional outcome of T cells in the context of thymocyte selection and highlight the role of force in mediating such interaction. These new findings add to and refine existing models of TCR triggering, but our understanding on the whole process of TCR triggering is far from complete. With these new information, more questions are generated.

Conformational change occurring at the transmembrane portion of CD3 has been reported previous (9), but what sequence of events lead to this conformational change is still unclear. It is likely that changes in the transmembrane region occurs due to force exertion on the extracellular site originated from TCR-pMHC interaction, but more direct evidence connecting these two events needs to be established. Going beyond the transmembrane region, dissociation of CD3 cytoplasmic tails from the plasma membrane

has long been suggested to be a direct consequence of TCR ligation (27). What is the role of force in CD3 tail dissociation? If the extracellular interaction between TCR-CD3 serves as a relay of mechanical forces across the membrane, it is possible that applying a sustained force on TCR or CD3 can lead to the dissociation of CD3 tails from the membrane. Single-molecule imaging, coupled with a direct method of monitoring force (i.e. through DNA force probes) or applying forces on specific surface molecules (i.e. through BFP assay) could unravel the direct relationship between force and CD3 tail dissociation. It would be beneficial to experiment with various TCR mutations aimed at affecting TCR-CD3 mutation to investigate the consequences of scenarios where the relay of force signals get disrupted.

Pertaining to thymocyte selection, it is still unclear how does TCR differentiate different peptides prior to CD8 engagement to MHC. Docking geometries and interaction kinetics are both possible candidates, although our findings showed comparable lifetime of TCR-pMHC interaction for ligands near the threshold either with or without force. TCR-pMHC interaction on thymocyte is also different from that on naïve T cells, as the latter forms catch-slip bond with agonist pMHCs without CD8 participation (13). What are the causes of these differences on the level of pMHC recognition? To further advance our understanding on TCR triggering and stay relevant to physiological conditions, we also need to probe into the role of self pMHCs. Since T cell naturally needs to discern its antigen from a large number of self-peptides, the contribution of other MHC molecules to TCR triggering warrants more attention. Even though MHCs loaded with self-peptides are not expected to interact with TCR, they can still form interaction with coreceptors. Taking into consideration the inside-out arm of TCR signaling, association of Lck to CD3 keeps

CD8 close to the TCR complex, which gives rise to the possibility for CD8 to bind to other neighboring MHCs, many of them are those carrying self-peptides under physiological conditions. In addition, a TCR complex is not restricted to one CD8 coreceptor, making it very likely that CD8 binding to MHC can bridge multiple MHC molecules together and even contribute to TCR aggregation.

REFERENCES

1. Duan S & Thomas PG (2016) Balancing Immune Protection and Immune Pathology by CD8(+) T-Cell Responses to Influenza Infection. *Front Immunol* 7:25.

2. Adams JJ*, et al.* (2016) Structural interplay between germline interactions and adaptive recognition determines the bandwidth of TCR-peptide-MHC cross-reactivity. *Nat Immunol* 17(1):87-94.

3. Alam SM*, et al.* (1999) Qualitative and quantitative differences in T cell receptor binding of agonist and antagonist ligands. *Immunity* 10(2):227-237.

4. Rosette C*, et al.* (2001) The impact of duration versus extent of TCR occupancy on T cell activation: a revision of the kinetic proofreading model. *Immunity* 15(1):59-70.

5. Huang J*, et al.* (2010) The kinetics of two-dimensional TCR and pMHC interactions determine T-cell responsiveness. *Nature* 464(7290):932-936.

6. Kuhns MS & Davis MM (2012) TCR Signaling Emerges from the Sum of Many Parts. *Front Immunol* 3:159.

7. Wegener AM, Hou X, Dietrich J, & Geisler C (1995) Distinct domains of the CD3-gamma chain are involved in surface expression and function of the T cell antigen receptor. *J Biol Chem* 270(9):4675-4680.

8. Wucherpfennig KW, Gagnon E, Call MJ, Huseby ES, & Call ME (2010) Structural biology of the T-cell receptor: insights into receptor assembly, ligand recognition, and initiation of signaling. *Cold Spring Harb Perspect Biol* 2(4):a005140.

9. Lee MS*, et al.* (2015) A Mechanical Switch Couples T Cell Receptor Triggering to the Cytoplasmic Juxtamembrane Regions of CD3zetazeta. *Immunity* 43(2):227-239.

10. Hu KH & Butte MJ (2016) T cell activation requires force generation. *J Cell Biol* 213(5):535-542.

11. Dustin ML (2008) T-cell activation through immunological synapses and kinapses. *Immunol Rev* 221:77-89.

12. Ilani T, Vasiliver-Shamis G, Vardhana S, Bretscher A, & Dustin ML (2009) T cell antigen receptor signaling and immunological synapse stability require myosin IIA. *Nat Immunol* 10(5):531-539.

13. Liu B, Chen W, Evavold BD, & Zhu C (2014) Accumulation of dynamic catch bonds between TCR and agonist peptide-MHC triggers T cell signaling. *Cell* 157(2):357-368.

14. Kane LP, Lin J, & Weiss A (2000) Signal transduction by the TCR for antigen. *Curr Opin Immunol* 12(3):242-249.

15. Lewis RS (2001) Calcium signaling mechanisms in T lymphocytes. *Annu Rev Immunol* 19:497-521.

16. Kim ST*, et al.* (2009) The alphabeta T cell receptor is an anisotropic mechanosensor. *J Biol Chem* 284(45):31028-31037.

17. Li YC*, et al.* (2010) Cutting Edge: mechanical forces acting on T cells immobilized via the TCR complex can trigger TCR signaling. *J Immunol* 184(11):5959-5963.

18. Marzio R, Mauel J, & Betz-Corradin S (1999) CD69 and regulation of the immune function. *Immunopharmacol Immunotoxicol* 21(3):565-582.

19. Ghendler Y, Smolyar A, Chang HC, & Reinherz EL (1998) One of the CD3epsilon subunits within a T cell receptor complex lies in close proximity to the Cbeta FG loop. *J Exp Med* 187(9):1529-1536.

20. Garcia KC*, et al.* (1996) An alphabeta T cell receptor structure at 2.5 A and its orientation in the TCR-MHC complex. *Science* 274(5285):209-219.

21. Birnbaum ME*, et al.* (2014) Molecular architecture of the alphabeta T cell receptor-CD3 complex. *Proc Natl Acad Sci U S A* 111(49):17576-17581.

22. Kuhns MS & Davis MM (2007) Disruption of extracellular interactions impairs T cell receptor-CD3 complex stability and signaling. *Immunity* 26(3):357-369.

23. Call ME, Pyrdol J, Wiedmann M, & Wucherpfennig KW (2002) The organizing principle in the formation of the T cell receptor-CD3 complex. *Cell* 111(7):967-979.

24. Sun ZY*, et al.* (2004) Solution structure of the CD3epsilondelta ectodomain and comparison with CD3epsilongamma as a basis for modeling T cell receptor topology and signaling. *Proc Natl Acad Sci U S A* 101(48):16867-16872.

25. Kuhns MS, Davis MM, & Garcia KC (2006) Deconstructing the form and function of the TCR/CD3 complex. *Immunity* 24(2):133-139.

26. Natarajan A*, et al.* (2016) Structural Model of the Extracellular Assembly of the TCR-CD3 Complex. *Cell Rep* 14(12):2833-2845.

27. Xu C*, et al.* (2008) Regulation of T cell receptor activation by dynamic membrane binding of the CD3epsilon cytoplasmic tyrosine-based motif. *Cell* 135(4):702-713.

28. Shi X, *et al.* (2013) Ca2+ regulates T-cell receptor activation by modulating the charge property of lipids. *Nature* 493(7430):111-115.

29. Marshall BT, *et al.* (2003) Direct observation of catch bonds involving cell-adhesion molecules. *Nature* 423(6936):190-193.

30. Kong F, Garcia AJ, Mould AP, Humphries MJ, & Zhu C (2009) Demonstration of catch bonds between an integrin and its ligand. *J Cell Biol* 185(7):1275-1284.

31. Chen W, Lou J, & Zhu C (2010) Forcing switch from short- to intermediate- and long-lived states of the alphaA domain generates LFA-1/ICAM-1 catch bonds. *J Biol Chem* 285(46):35967-35978.

32. Yago T, *et al.* (2008) Platelet glycoprotein Ibalpha forms catch bonds with human WT vWF but not with type 2B von Willebrand disease vWF. *J Clin Invest* 118(9):3195-3207.

33. Germain RN (2002) T-cell development and the CD4-CD8 lineage decision. *Nat Rev Immunol* 2(5):309-322.

34. Godfrey DI, Kennedy J, Suda T, & Zlotnik A (1993) A developmental pathway involving four phenotypically and functionally distinct subsets of CD3-CD4-CD8-triple-negative adult mouse thymocytes defined by CD44 and CD25 expression. *J Immunol* 150(10):4244-4252.

35. Groettrup M, *et al.* (1993) A novel disulfide-linked heterodimer on pre-T cells consists of the T cell receptor beta chain and a 33 kd glycoprotein. *Cell* 75(2):283-294.

36. Robey E & Fowlkes BJ (1994) Selective events in T cell development. *Annu Rev Immunol* 12:675-705.

37. von Boehmer H, Teh HS, & Kisielow P (1989) The thymus selects the useful, neglects the useless and destroys the harmful. *Immunol Today* 10(2):57-61.

38. Evavold BD, Sloan-Lancaster J, & Allen PM (1993) Tickling the TCR: selective T-cell functions stimulated by altered peptide ligands. *Immunol Today* 14(12):602-609.

39. Gao GF, *et al.* (1997) Crystal structure of the complex between human CD8alpha(alpha) and HLA-A2. *Nature* 387(6633):630-634.

40. Kern PS, *et al.* (1998) Structural basis of CD8 coreceptor function revealed by crystallographic analysis of a murine CD8alphaalpha ectodomain fragment in complex with H-2Kb. *Immunity* 9(4):519-530.

41. Garcia KC, *et al.* (1996) CD8 enhances formation of stable T-cell receptor/MHC class I molecule complexes. *Nature* 384(6609):577-581.

42. Laugel B, *et al.* (2007) Different T cell receptor affinity thresholds and CD8 coreceptor dependence govern cytotoxic T lymphocyte activation and tetramer binding properties. *J Biol Chem* 282(33):23799-23810.

43. Davis MM, *et al.* (2003) Dynamics of cell surface molecules during T cell recognition. *Annu Rev Biochem* 72:717-742.

44. Casas J, *et al.* (2014) Ligand-engaged TCR is triggered by Lck not associated with CD8 coreceptor. *Nat Commun* 5:5624.

45. Delon J, *et al.* (1998) CD8 expression allows T cell signaling by monomeric peptide-MHC complexes. *Immunity* 9(4):467-473.

46. Wyer JR, *et al.* (1999) T cell receptor and coreceptor CD8 alphaalpha bind peptide-MHC independently and with distinct kinetics. *Immunity* 10(2):219-225.

47. Jiang N, *et al.* (2011) Two-stage cooperative T cell receptor-peptide major histocompatibility complex-CD8 trimolecular interactions amplify antigen discrimination. *Immunity* 34(1):13-23.

48. Wang X & Ha T (2013) Defining single molecular forces required to activate integrin and notch signaling. *Science* 340(6135):991-994.

49. Luca VC, *et al.* (2017) Notch-Jagged complex structure implicates a catch bond in tuning ligand sensitivity. *Science* 355(6331):1320-1324.

50. Zhang Y, Ge C, Zhu C, & Salaita K (2014) DNA-based digital tension probes reveal integrin forces during early cell adhesion. *Nat Commun* 5:5167.

51. Liu Y, *et al.* (2016) DNA-based nanoparticle tension sensors reveal that T-cell receptors transmit defined pN forces to their antigens for enhanced fidelity. *Proc Natl Acad Sci U S A* 113(20):5610-5615.

52. Blakely BL, *et al.* (2014) A DNA-based molecular probe for optically reporting cellular traction forces. *Nat Methods* 11(12):1229-1232.

53. Ma VP, *et al.* (2016) Ratiometric Tension Probes for Mapping Receptor Forces and Clustering at Intermembrane Junctions. *Nano Lett* 16(7):4552-4559.

54. O'Shea EK, Lumb KJ, & Kim PS (1993) Peptide 'Velcro': design of a heterodimeric coiled coil. *Curr Biol* 3(10):658-667.

55. Kjer-Nielsen L, *et al.* (2003) A structural basis for the selection of dominant alphabeta T cell receptors in antiviral immunity. *Immunity* 18(1):53-64.

56. Kjer-Nielsen L, *et al.* (2004) Crystal structure of the human T cell receptor CD3 epsilon gamma heterodimer complexed to the therapeutic mAb OKT3. *Proc Natl Acad Sci U S A* 101(20):7675-7680.

57. Sun ZJ, Kim KS, Wagner G, & Reinherz EL (2001) Mechanisms contributing to T cell receptor signaling and assembly revealed by the solution structure of an ectodomain fragment of the CD3 epsilon gamma heterodimer. *Cell* 105(7):913-923.

58. Newell EW*, et al.* (2011) Structural basis of specificity and cross-reactivity in T cell receptors specific for cytochrome c-I-E(k). *J Immunol* 186(10):5823-5832.

59. Daniels MA*, et al.* (2006) Thymic selection threshold defined by compartmentalization of Ras/MAPK signalling. *Nature* 444(7120):724-729.

60. Hogquist KA*, et al.* (1997) Identification of a naturally occurring ligand for thymic positive selection. *Immunity* 6(4):389-399.

61. Santori FR*, et al.* (2002) Rare, structurally homologous self-peptides promote thymocyte positive selection. *Immunity* 17(2):131-142.

62. Nathenson SG, Geliebter J, Pfaffenbach GM, & Zeff RA (1986) Murine major histocompatibility complex class-I mutants: molecular analysis and structure-function implications. *Annu Rev Immunol* 4:471-502.

63. Tallquist MD, Yun TJ, & Pease LR (1996) A single T cell receptor recognizes structurally distinct MHC/peptide complexes with high specificity. *J Exp Med* 184(3):1017-1026.

64. Kuhns ST, Tallquist MD, Johnson AJ, Mendez-Fernandez Y, & Pease LR (2000) T cell receptor interactions with class I heavy-chain influence T cell selection. *Proc Natl Acad Sci U S A* 97(2):756-760.

65. Degano M*, et al.* (2000) A functional hot spot for antigen recognition in a superagonist TCR/MHC complex. *Immunity* 12(3):251-261.

66. Pawlowski TJ, Singleton MD, Loh DY, Berg R, & Staerz UD (1996) Permissive recognition during positive selection. *Eur J Immunol* 26(4):851-857.

67. Sauer K, Huang YH, Lin H, Sandberg M, & Mayr GW (2009) Phosphoinositide and inositol phosphate analysis in lymphocyte activation. *Curr Protoc Immunol* Chapter 11:Unit11 11.

68. Puls KL, Hogquist KA, Reilly N, & Wright MD (2002) CD53, a thymocyte selection marker whose induction requires a lower affinity TCR-MHC interaction than CD69, but is up-regulated with slower kinetics. *Int Immunol* 14(3):249-258.

69. Chesla SE, Selvaraj P, & Zhu C (1998) Measuring two-dimensional receptor-ligand binding kinetics by micropipette. *Biophys J* 75(3):1553-1572.

70. Evans E, Berk D, & Leung A (1991) Detachment of agglutinin-bonded red blood cells. I. Forces to rupture molecular-point attachments. *Biophys J* 59(4):838-848.

71. Chen W, Zarnitsyna VI, Sarangapani KK, Huang J, & Zhu C (2008) Measuring Receptor-Ligand Binding Kinetics on Cell Surfaces: From Adhesion Frequency to Thermal Fluctuation Methods. *Cell Mol Bioeng* 1(4):276-288.

72. Chen W, Evans EA, McEver RP, & Zhu C (2008) Monitoring receptor-ligand interactions between surfaces by thermal fluctuations. *Biophys J* 94(2):694-701.

73. Chen W, Lou J, Evans EA, & Zhu C (2012) Observing force-regulated conformational changes and ligand dissociation from a single integrin on cells. *J Cell Biol* 199(3):497-512.

74. Germain RN & Stefanova I (1999) The dynamics of T cell receptor signaling: complex orchestration and the key roles of tempo and cooperation. *Annu Rev Immunol* 17:467-522.

75. Irvine DJ, Purbhoo MA, Krogsgaard M, & Davis MM (2002) Direct observation of ligand recognition by T cells. *Nature* 419(6909):845-849.

76. Cambier JC (1995) Antigen and Fc receptor signaling. The awesome power of the immunoreceptor tyrosine-based activation motif (ITAM). *J Immunol* 155(7):3281-3285.

77. He Y*, et al.* (2015) Identification of the Docking Site for CD3 on the T Cell Receptor beta Chain by Solution NMR. *J Biol Chem* 290(32):19796-19805.

78. Arnett KL, Harrison SC, & Wiley DC (2004) Crystal structure of a human CD3-epsilon/delta dimer in complex with a UCHT1 single-chain antibody fragment. *Proc Natl Acad Sci U S A* 101(46):16268-16273.

79. Rojo JM & Janeway CA, Jr. (1988) The biologic activity of anti-T cell receptor V region monoclonal antibodies is determined by the epitope recognized. *J Immunol* 140(4):1081-1088.

80. Boniface JJ*, et al.* (1998) Initiation of signal transduction through the T cell receptor requires the multivalent engagement of peptide/MHC ligands [corrected]. *Immunity* 9(4):459-466.

81. Krogsgaard M*, et al.* (2005) Agonist/endogenous peptide-MHC heterodimers drive T cell activation and sensitivity. *Nature* 434(7030):238-243.

82. Minguet S, Swamy M, Alarcon B, Luescher IF, & Schamel WW (2007) Full activation of the T cell receptor requires both clustering and conformational changes at CD3. *Immunity* 26(1):43-54.

83. van der Merwe PA & Dushek O (2011) Mechanisms for T cell receptor triggering. *Nat Rev Immunol* 11(1):47-55.

84. Chen W & Zhu C (2013) Mechanical regulation of T-cell functions. *Immunol Rev* 256(1):160-176.

85. Wang JH & Reinherz EL (2012) The structural basis of alphabeta T-lineage immune recognition: TCR docking topologies, mechanotransduction, and co-receptor function. *Immunol Rev* 250(1):102-119.

86. Ma Z, Janmey PA, & Finkel TH (2008) The receptor deformation model of TCR triggering. *FASEB J* 22(4):1002-1008.

87. Martinez-Martin N*, et al.* (2009) Cooperativity between T cell receptor complexes revealed by conformational mutants of CD3epsilon. *Sci Signal* 2(83):ra43.

88. Karaivanova V, Suzuki C, Howe C, & Kearse KP (1999) Characterization of the epitope on murine T-cell receptor (TCR) alpha proteins recognized by H28-710 monoclonal antibody. *Hybridoma* 18(6):497-503.

89. Touma M*, et al.* (2006) The TCR C beta FG loop regulates alpha beta T cell development. *J Immunol* 176(11):6812-6823.

90. Kuhns MS*, et al.* (2010) Evidence for a functional sidedness to the alphabetaTCR. *Proc Natl Acad Sci U S A* 107(11):5094-5099.

91. Mossman KD, Campi G, Groves JT, & Dustin ML (2005) Altered TCR signaling from geometrically repatterned immunological synapses. *Science* 310(5751):1191-1193.

92. Mallis RJ*, et al.* (2015) Pre-TCR ligand binding impacts thymocyte development before alphabetaTCR expression. *Proc Natl Acad Sci U S A* 112(27):8373-8378.

93. Das DK*, et al.* (2015) Force-dependent transition in the T-cell receptor beta-subunit allosterically regulates peptide discrimination and pMHC bond lifetime. *Proc Natl Acad Sci U S A* 112(5):1517-1522.

94. Wang H*, et al.* (2010) ZAP-70: an essential kinase in T-cell signaling. *Cold Spring Harb Perspect Biol* 2(5):a002279.

95. Huang J, Meyer C, & Zhu C (2012) T cell antigen recognition at the cell membrane. *Mol Immunol* 52(3-4):155-164.

96. Ma Z, Sharp KA, Janmey PA, & Finkel TH (2008) Surface-anchored monomeric agonist pMHCs alone trigger TCR with high sensitivity. *PLoS Biol* 6(2):e43.

97. Judokusumo E, Tabdanov E, Kumari S, Dustin ML, & Kam LC (2012) Mechanosensing in T lymphocyte activation. *Biophys J* 102(2):L5-7.

98. Husson J, Chemin K, Bohineust A, Hivroz C, & Henry N (Force generation upon T cell receptor engagement. *PLoS One* 6(5):e19680.

99. Bashour KT, *et al.* (2014) CD28 and CD3 have complementary roles in T-cell traction forces. *Proc Natl Acad Sci U S A* 111(6):2241-2246.

100. Pryshchep S, Zarnitsyna VI, Hong J, Evavold BD, & Zhu C (2014) Accumulation of serial forces on TCR and CD8 frequently applied by agonist antigenic peptides embedded in MHC molecules triggers calcium in T cells. *J Immunol* 193(1):68-76.

101. Hong J, *et al.* (2015) Force-Regulated In Situ TCR-Peptide-Bound MHC Class II Kinetics Determine Functions of CD4+ T Cells. *J Immunol* 195(8):3557-3564.

102. Lou J, *et al.* (2006) Flow-enhanced adhesion regulated by a selectin interdomain hinge. *J Cell Biol* 174(7):1107-1117.

103. Stepanek O, *et al.* (2014) Coreceptor Scanning by the T Cell Receptor Provides a Mechanism for T Cell Tolerance. *Cell*.

104. Fiore VF, Ju L, Chen Y, Zhu C, & Barker TH (2014) Dynamic catch of a Thy-1-alpha5beta1+syndecan-4 trimolecular complex. *Nat Commun* 5:4886.

105. Hailman E & Allen PM (2005) Inefficient cell spreading and cytoskeletal polarization by CD4+CD8+ thymocytes: regulation by the thymic environment. *J Immunol* 175(8):4847-4857.

106. Hailman E, Burack WR, Shaw AS, Dustin ML, & Allen PM (2002) Immature CD4(+)CD8(+) thymocytes form a multifocal immunological synapse with sustained tyrosine phosphorylation. *Immunity* 16(6):839-848.

107. Kong F, *et al.* (2013) Cyclic mechanical reinforcement of integrin-ligand interactions. *Mol Cell* 49(6):1060-1068.

108. Hammer JA, 3rd & Burkhardt JK (2013) Controversy and consensus regarding myosin II function at the immunological synapse. *Curr Opin Immunol* 25(3):300-306.

109. Hwang S, *et al.* (2012) Reduced TCR signaling potential impairs negative selection but does not result in autoimmune disease. *J Exp Med* 209(10):1781-1795.

110. Hwang S, *et al.* (2015) TCR ITAM multiplicity is required for the generation of follicular helper T-cells. *Nat Commun* 6:6982.

111. Stepanek O, *et al.* (2014) Coreceptor scanning by the T cell receptor provides a mechanism for T cell tolerance. *Cell* 159(2):333-345.

112. Artyomov MN, Lis M, Devadas S, Davis MM, & Chakraborty AK (2010) CD4 and CD8 binding to MHC molecules primarily acts to enhance Lck delivery. *Proc Natl Acad Sci U S A* 107(39):16916-16921.